Study on corrosion properties of WC-Ni cold spray coatings to mitigate flow-accelerated corrosion of carbon steels in nuclear power plants

Jeongwon Kim
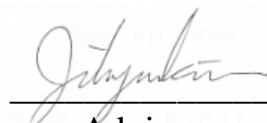
Department of Nuclear Engineering

Graduate School of UNIST

Study on corrosion properties of WC-Ni cold spray coatings to mitigate flow-accelerated corrosion of carbon steels in nuclear power plants

A thesis
submitted to the Graduate School of UNIST
in partial fulfillment of the
requirements for the degree of
Master of Science
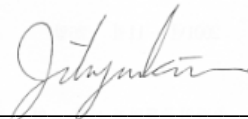
Jeongwon Kim

07/19/2016
Approved by

_____
Advisor
Ji Hyun Kim

Study on corrosion properties of WC-Ni cold spray coatings to mitigate flow-accelerated corrosion of carbon steels in nuclear power plants

Jeongwon Kim

This certifies that the thesis of Jeongwon Kim is approved.

07/19/2016

_____
Advisor: Ji Hyun Kim

_____
Snagjoon Ahn: Thesis Committese Member #1

_____
Sungyeol Choi: Thesis Committee Member #2

Study on corrosion properties of WC-Ni cold spray coatings to mitigating flow-accelerated corrosion of carbon steels in nuclear power plants

Jeongwon Kim

Department of Nuclear Engineering

The Graduate School

Ulsan National Institute of Science and Technology

In secondary system of pressurized water reactors (PWRs), carbon steel undergoes severe corrosion owing to high temperature and pressure, and fast flow velocity. These circumstance, named as flow-accelerated corrosion (FAC), induces corrosion and eventually failure of power piping. Flow velocity brings about destruction of oxide layer by electrochemical corrosion and mechanical shear stress at the oxide/water interfaces. The piping system in the secondary circuit of PWRs mainly consists of carbon steels being vulnerable to FAC because Fe, main element of carbon steel, forms Fe_3O_4 dissolved to secondary water system by changing to Fe ion.

To mitigate corrosion of carbon steel, chemical and mechanical treatments to carbon steel or changing secondary water chemistry has been widely studied. Addition of Cr and/or Mo to carbon steel components is one of the adequate countermeasure to mitigate FAC by anodic passivation. Mechanical treatments are controlling surface roughness because reducing surface roughness can decrease flow turbulence at the oxide/water interface. Increasing pH, dissolved oxygen contents, and addition of advanced corrosion inhibitor to secondary system can decrease corrosion rate of carbon steels. However, maintaining homogeneous chemistry condition of water is hardly possible and changing chemical composition of carbon steel needs not only research of corrosion properties but also other mechanical properties.

In contrast, application of coatings to the steel surface can be easily applied to the secondary system. Therefore, thermal spray to steel surface using less corrosive metal is widely used. Among them, cold spray has advantage with lower process temperature than that of other spray coatings which leads to low residual stress and oxidation or decarburization of coating.

In this study, tungsten carbide (WC) and nickel (Ni) particles are used as feedstock materials for the coating. WC exhibits high corrosion resistance in acidic aqueous media due to the phase stability.

Moreover, the oxidation resistance of WC in O_2 containing atmosphere at high temperature is applied to industry which is exposed to severe corrosive environments However, in alkaline solution, the dissolution of WC increases by forming WO^{4-}. Moreover, high melting temperature and poor plastic deformation make cold spray coating difficult. To suppress the corrosion of and increase the deposition efficiency of the coating, Ni, which has better plastic deformation and lower corrosion potential and melting temperature than WC, is used as a binder metal. Ni acts like a sacrificial metal to WC so corrosion and oxidation of Ni occur before those of WC.

To evaluate the potential of the coating as an effective corrosion barrier, series of corrosion tests at simulated secondary water chemistry is carried out and quantitative analysis is conducted. Surface and cross-section morphologies of the coatings before and after FAC simulation tests is investigated by scanning electron microscope and X-ray photoelectron microscopy. Electrochemical experiments are carried out for quantitative analysis.

Cold spray coatings using WC-10Ni with different Ni contents have rough and porous surface but significant changes of surface is not observed by SEM image. However, lower current density is measured at 25Ni coating than carbon steel, P22, 20Ni and 30Ni coating from potentiodynamic polarization experiments in pH 9.3 ETA solution at room temperature. After 2 weeks FAC experiments, weight loss of coating is increased with increases Ni contents in coating but weight of 20Ni coating is increased. On the other hands, weight loss occurs at 20Ni and 30Ni coating and weight of 25Ni coating is increased after 4 weeks FAC experiments. Although weight change of coatings is smaller than carbon steel after 2 weeks and 4 weeks FAC experiments, weight change of 25Ni coating shows better corrosion performance than P22 comparing with 20Ni and 30Ni coating.

As a result, Ni has lower corrosion potential than WC and it induces galvanic corrosion of Ni and prevents WC corrosion or oxidation at early stage of corrosion process. Moreover, oxidation product of Ni, $Ni(OH)_2$ is dissolved into water by Ni ion because of poor thermal stability of $Ni(OH)_2$. Therefore, high Ni contents in coating increases weight loss during the early stages by $Ni(OH)_2$ dissolution. However, after 4 weeks of immersion, WC oxidizes and transforms into WO_3 increasingly which is influenced by Ni contents. 30Ni coating induces continuous weight loss during FAC simulation because of low WC contents which means weight gain by WO_3 formation is smaller than weight loss by $Ni(OH)_2$ dissolution. Therefore, weight loss occurs at 30Ni coating. Contrarily, 20Ni coating do not protect WC dissolution after 2 weeks because the absence of Ni and $Ni(OH)_2$.accelerates WC oxidation and WO_3 dissolution to water.

To be concluded, WC-10Ni + 25Ni coating specimens exhibit the best corrosion resistive performance, the lower corrosion current density and the small weight change than other coatings. Therefore, WC-10Ni + 25Ni coating is possibly suggested to one of the option to mitigate corrosion of carbon steels.

Contents

List of figures

7

List of tables

I. Introduction

1.1 Background of research

Fe-based material is used as structural materials that hold the interior of the building and protect the outside of the material or the pipe. Among them, carbon steel has mechanical and economical advantages. In the field of nuclear power plant, carbon steel can be used in the internal structure or material of the pipe that water flows continuously. In particular, secondary system of nuclear power plant is made up of steel pipes about hundreds of kilometers so carbon steel is mainly used due to the advantage about the cost aspects [1].

Secondary system in nuclear power plant is a structure to produce electricity by transform thermal energy of steam to kinetic energy of turbine. The energy of steam is produced from primary system, nuclear reactor, which makes thermal energy from the fission of nuclear fuel. Therefore, to promote thermal efficiency, high temperature of water is needed. Thus, secondary system needs high pressure, and high temperature for electricity efficiency. However, metal is exposed to a risk of a corrosion which decreases mechanical properties such as hardness or toughness etc. and electrochemical properties such as a resistance to corrosion [2].

Fe contacts with specific environments of the water which is high pH, high temperature, high pressure and fast flow velocity in secondary system of nuclear power plant. As a result, the interior of the pipe transforms into corrosion products, and these products dissolves into bulk water constantly due to the chemical condition with high velocity. Therefore, the metallic substrate is exposed to water continuously because passive layer is not formed stably at metal/water interface. These phenomena accelerate wall thinning of the pipe, especially carbon steel or low alloy steel, and denominates flow-accelerated corrosion (FAC) [3]. Unlike primary system inside the containment, a pipe rupture of secondary system has possibility about casualties so the effort is necessary to avoid FAC. Many accidents due to FAC occurring at nuclear power plants around the world and other industry producing electricity has a problem about these phenomena. The accidents cases by FAC at nuclear power plant is in Table 1.1.

1.2 Objectives

To prevent the accidents mentioned above, the researches to enhance the corrosion resistance of the pipe have been carried out in many laboratory or industry. In this study, corrosion of carbon steel is investigated experimentally when other material is coated to steel's surface by cold spray coating. Prior to the actual coating to the inside of the pipe, a coated steel plate is used to observe corrosion properties at similar conditions with secondary system of nuclear power plant. By this study, appropriate chemical composition of cold spray coating is investigated and coating can be a one of the methods for mitigating FAC of carbon steel.

Table. 1.1 Events caused by FAC at power plant [4]

Plant	Type	Date	System
Surry	PWR	1986.12	Condensate
Trojan	PWR	1987.6	Feedwater
Santa Maria de Garona	BWR	1989.12	Feedwater
Millstone 3	PWR	1990.12	Separator drain
Millstone 2	PWR	1995.08	Heater drain
Mihama 3	PWR	2004.08	Feedwater

II. Literature study

2.1 Definition of flow-accelerated corrosion

FAC is metal degradation at water condition by fast flow velocity, high temperature, high pressure and high pH but it occurs at the other energy production system which uses water and steam to move turbine for electricity as well as nuclear power plant. Contrary to metal oxidation, FAC causes oxide dissolution inducing wall thinning [3, 5]. The reason of this phenomenon is thermodynamic stability of iron, main component of carbon steel, so carbon steel and low alloy steel are vulnerable to FAC.

Fig. 2.1 is Pourbaix diagram of iron at 25 °C constructed by HSC 6.0 and Fig. 2.2 shows iron stability at various pH and potential at 150 ℃. Iron solubility comes from B. Beverskog et al., and these solubility is experimental results (5 13 $*10^{-2}$ mol/kg at 25°C and $1.5*10^{-6}$ mol/kg at 150°C). At ambient temperature, iron hydroxide and magnetite (Fe_3O_4) is stable formation of iron but at the operating temperature of secondary system, Fe_3O_4 dissolution can be significantly increased because of $Fe(OH)^+$ transformation by hydrogen from metal-oxide interface.

Equations of FAC [7] are:

$$Fe + 2H_2O \rightarrow Fe^{2+} + 2OH^- + H_2 \tag{1}$$

$$Fe + 2H_2O \rightarrow Fe(OH)_2 + H_2 \tag{2}$$

$$Fe^{2+} + 2OH^- \leftrightarrow Fe(OH)_2 \tag{3}$$

$$3Fe + 4H_2O \rightarrow Fe_3O_4 + 4H_2 \tag{4}$$

$$\frac{1}{3}Fe_3O_4 + (2-b)H^+ + \frac{1}{3}H_2 \rightarrow Fe(OH)_b^{(2-b)+} + \left(\frac{4}{3}-b\right)H_2O \tag{5}$$
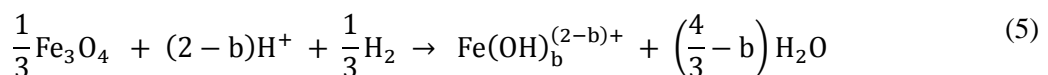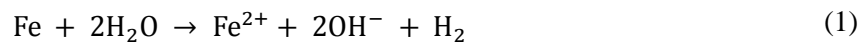
Carbon steel has passive layer such as Fe_3O_4 iron hydroxide ($Fe(OH)_2$) or hematite (Fe_2O_3) at circumstance which doesn't have high flow velocity or that has low temperature and high pH. And this mechanism is supported by equation (2), (3) and (4) and Fig. 2.1. However, corrosive environment like

a secondary water chemistry in nuclear power plant transforms Fe_3O_4 to iron ion and leads dissolution to water continuously. Equation (5) and Fig. 2.2 mean Fe_3O_4 reacts with hydrogen at oxide-water interface and is dissolved to water.

Fig. 2.3 is schematic of the Fe_3O_4 dissolution of FAC. Oxide instability leads $Fe(OH)^+$ dissolution and increasing porosity at Fe_3O_4 film [9]. Therefore, porous Fe_3O_4 layer acts like a corrosion activation site which accelerates dissolution and carbon steel is exposed to water [10]. As a results, thickness of carbon steel pipe is much thinner and thinner. Eventually, a pipe rupture can occur by pressure of water.

2.2 Main factor of flow-accelerated corrosion

2.2.1 Flow velocity

Flow velocity as a factor for determining the properties of the fluid separates flow into a laminar and turbulent flow. The separation is determined by the Reynolds number which is ratio of inertial forces to viscous forces. The critical Reynolds number for transition laminar and turbulent flow is between 2300 and 4000 [11] but it can be different by other factor. In equation (6),

$$Re = \frac{\rho_f \upsilon_f d}{\mu} \qquad (6)$$

Where ρ_f is density of fluid and υ_f is velocity of fluid and d is characteristic length and μ is dynamic viscosity, Reynolds number increases with increasing fluid velocity which means high flow velocity induces turbulent condition [12].

The reason for importance of Reynolds number is that the dimensionless number, Re, is proportional to mass transfer coefficient (MTC). MTC determines transport from oxide or metal–water interface to water at secondary water chemistry. Mechanism model of FAC expressed by MTC [7] is from Fick's law of diffusion and equation (7)

$$FAC\ rate = MTC\ (C_w - C_b) \qquad (7)$$

The concentration difference between metal-water interface and bulk water raises diffusion rate and

14

FAC rate. The relationship between MTC and Reynolds number is expressed by equation (8)

$$Sh = a * Re^b * Sc^c = \frac{MTC * d_H}{D} \tag{8}$$

Moreover, high flow velocity decreases concentration at bulk solution so corrosion rate is dramatically increased.

Experimental result in Fig. 2.4 was carried out for observing electrode rotation. Comparing stationary test, rotating electrode experiments maintains high current density, approximately 0.5 mA/cm^2 after 300 seconds. Contrary to rotating test, stationary test has low current density after 600 seconds. However, in rotating test, flow velocity made by rotating increases dissolution of iron oxide and increases current density.

MTC was sharply increased above 4m/s and the laminar flow and the turbulent flow is divided by flow velocity, 4 m/s. Fig. 2.5 shows that flow velocity raises mass transfer coefficient and transforms flow condition from a laminar to a turbulent condition experimentally. Mentioned above at equation (7), magnitude of corrosion rate is different between laminar and turbulent flow. Increasing rate of metal loss at Fig. 2.6 is small at a laminar flow but gradient mass loss per mass coefficient is larger than a laminar condition at a turbulent condition. Figs. 2.5 and 2.6 mean that high flow velocity raises Reynolds number and mass transfer coefficient which induces increasing corrosion rate.

2.2.2 Temperature

Temperature affects metal loss by FAC and influences on the other factor, pH, Reynolds number, viscosity of fluid, density or iron solubility. For example, hydrogen solubility is increased with temperature increases so alkaline solution at room temperature can change to basic solution at high temperature. Effect of temperature on pH is explained at Fig. 2.7. Decreases pH at high temperature result in Fe_3O_4 dissolution by hydrogen and weight loss of carbon steel is increased.

In the point of view of solubility of iron, FAC rate is the product of MTC and concentration difference of iron. And corrosion rate is converted to the product of MTC and solubility of iron with assumption that concentration of bulk solution is zero. However, solubility of iron and MTC are inversely related to each other. Kinematic viscosity of water at room temperature is higher than that of water at high temperature and ion diffusivity is low because low temperature generates low energy to diffusion.

15

Therefore, MTC at low temperature is smaller than high temperature. However, solubility of iron to water decreases with increasing temperature. Therefore, FAC rate governed by temperature has bell shape which is result of production MTC with solubility.

2.2.3 pH

Iron oxide, especially Fe_3O_4, reacts with hydrogen ion at low pH condition which means the concentration of hydrogen is high. In equation (3) and (5), Fe_3O_4 is converted to $Fe(OH)^+$ or Fe^{2+} finally [3, 5]. Pourbaix diagram at 150 °C of water, Fig. 2.2, shows that Fe_3O_4 is stable form of iron at -0.5 corrosion potential and pH 7 region. However, with decreasing pH, Fe^{2+} and $Fe(OH)^+$ is dominant iron species and stable. Therefore, high pH condition is needed to stabilize Fe_3O_4 that does not dissolve into the water [10].

2.2.4 Dissolved oxygen

Effect of dissolved oxygen (DO) in water was investigated in many literature and corrosion of carbon steel is decreased by increasing oxygen contents. Specifically, in pH 7 neutral solution, significant change of corrosion rate is not observed below 10 ppb but metal loss at condition above 50 ppb was decreased significantly and researcher considered that FAC did not occur.

Although low oxygen contents cannot prohibit corrosion and dissolution of iron, high oxygen contents transform Fe_3O_4, to Fe_2O_3 which has low solubility to water. Iron solubility to water of Fe_3O_4 is 10^{-6} mol/kg but solubility of iron is decreased to 10^{-12} mol/kg in case of Fe_2O_3 [14].

Also, electrochemical corrosion potential (ECP) at 50 ppb and 100 ppb condition in Fig. 2.10 is different from that of 1 to 10 ppb condition. Increasing of ECP means stability formation of specimens can be different by analyzing Pourbaix diagram. ECP at 1 to 10 ppb condition is formed at region between -0.4 V and 0.6 V. Therefore, iron ion is dominant in the circumstance because Pourbaix diagram at Fig. 2.1 represents iron ion is stable and dissolves to water at pH 7 and -0.5 V condition. On the other hands, high DO raises ECP above -0.2 V and iron is transformed to Fe_2O_3 and dissolution of iron is decreased so difference of corrosion rate occurs. Therefore, existence of oxygen in water influences on decreasing corrosion rate because Fe_2O_3 is created at porous oxide film which consists of Fe_3O_4. Fe_2O_3 formation occurs according to the following equation (9)

$$\text{Fe(OH)}_2 + \frac{1}{2}O_2 \leftrightarrow \text{Fe}_2\text{O}_3 + 2\text{H}_2\text{O} \qquad (9)$$
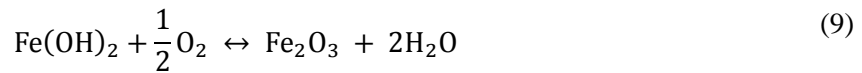
2.2.5 Roughness

Physical difference such as surface roughness effects on corrosion properties of steel. A rough surface contacts with severe condition and these protruding areas have low activation energy. Therefore, corrosion more easily occur than smooth surface. In experimental research, surface roughness tended to be decreased at Fig. 2.11 which indicated iron at protruding areas dissolved to water and these area was smoother than before.

Fig. 2.12 shows other effect of roughness to change of flow condition. Over all, flow is in laminar condition but protruding edges interferes flow direction. This effect induces turbulent eddy at metal-water interface which accelerates corrosion rate because corrosion rate is increased at turbulent condition.

2.3 Methods for mitigating flow-accelerated corrosion

A lots of researcher has studied about the methods for preventing FAC and electrochemical and mechanical methods are studied.

First, an electrochemical method is divided to two solutions which are change of water chemistry or steel components. In case of water chemistry, low contents of hydrogen ion indicate reaction rate of Fe_3O_4 at equation (5) is reduced and therefore high pH condition can suppress metal degradation at secondary system of nuclear power plant. When the temperature of water which is pH 9 at room temperature is raised above 150℃, the production of MTC and the concentration of iron is decreased and this results can influence on equation (7) so damages by flow accelerated corrosion are reduced by increasing operation temperature. Another option is decreasing iron solubility to water by oxygen concentration. Oxygen in water promotes Fe_2O_3 production than Fe_3O_4 and Fe_2O_3 formation can reduce iron dissolution to water. Therefore, high DO at secondary system is good process for decreasing corrosion rate of carbon steel pipe.

Cr addition to carbon steel change significantly Pourbaix diagram and iron solubility. Pourbaix diagram at Fig. 2.13 for Fe-Cr-H$_2$O indicates dominant component at secondary water chemistry is FeCr$_2$O$_4$.

17

These oxide reacts with hydrogen under following equation (10)

$$FeCr_2O_4 + H^+ \leftrightarrow FeOH^+ + Cr_2O_3 \tag{10}$$
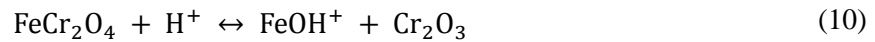
Therefore, iron solubility in abovementioned equation is $1.8 * 10^{-10}$ mol/kg at 200 °C. These value of $FeOH^+$ is smaller than Fe_3O_4 solubility, 10^{-6} mol/kg. So corrosion of carbon steel added Cr is suppressed.

Seconds, mechanical methods such as reducing surface roughness is the other option to suppress corrosion reaction with water. Smooth surface has small contacted area with water so the corrosion or oxidation with water is decreased. Moreover, local turbulent area has small fraction comparing all metal-water interface. It means corrosion accelerated by turbulent condition can be suppressed and corrosion rate is decreased.

2.4 Limitation of control flow-accelerated corrosion factor

Although alkaline condition is maintained at room temperature, pH is decreased with increasing temperature at high temperature because of high concentration of hydrogen ion at high temperature. This phenomenon is revealed at Fig. 2.7. Moreover, the pH difference at high temperature is dramatically smaller than that at room temperature. Therefore, increasing pH at room temperature cannot prohibit Fe_3O_4 dissolution perfectly.

Rectangular and circular data from Fig. 2.14 is iron concentration at pH 9 and pH 7 at room temperature. It indicates maximum FAC rate exists at various temperature. Secondary water condition is changed when fluid flows in pipe. Therefore, the most severe corrosive site at pipe is changed by flow temperature. As a results, control by changing temperature is excursive methods.

Changes a turbulent flow to a laminar flow influences thermodynamic problem between primary circuit and secondary system which is not a material issues.

Change or addition other elements needs other mechanical test for certification such as ASTM to applicate to the industrial sites as well as corrosion test. P22 as a substitutes of carbon steel is developed and used at nuclear power plant but Cr and Mo addition above 3 wt.% increase production cost and decreases price competitiveness.

At literature study, high DO decreases corrosion rate of carbon steel. Therefore, uses of fluid injected oxygen or continuous supplying the oxygen to water are methods for applying to nuclear industry.

However, the former methods cause FAC at the rear part which has low DO and the latter methods results in other corrosion phenomena at the site supplying oxygen.

Therefore, control FAC factor for mitigating FAC rate is difficult and is not an essential solution for corrosion protection.

Eh (Volts)

Fe - H2O - System at 25.00 C

Fig. 2.1 Fe Pourbaix diagram at 25 °C

Eh (Volts)
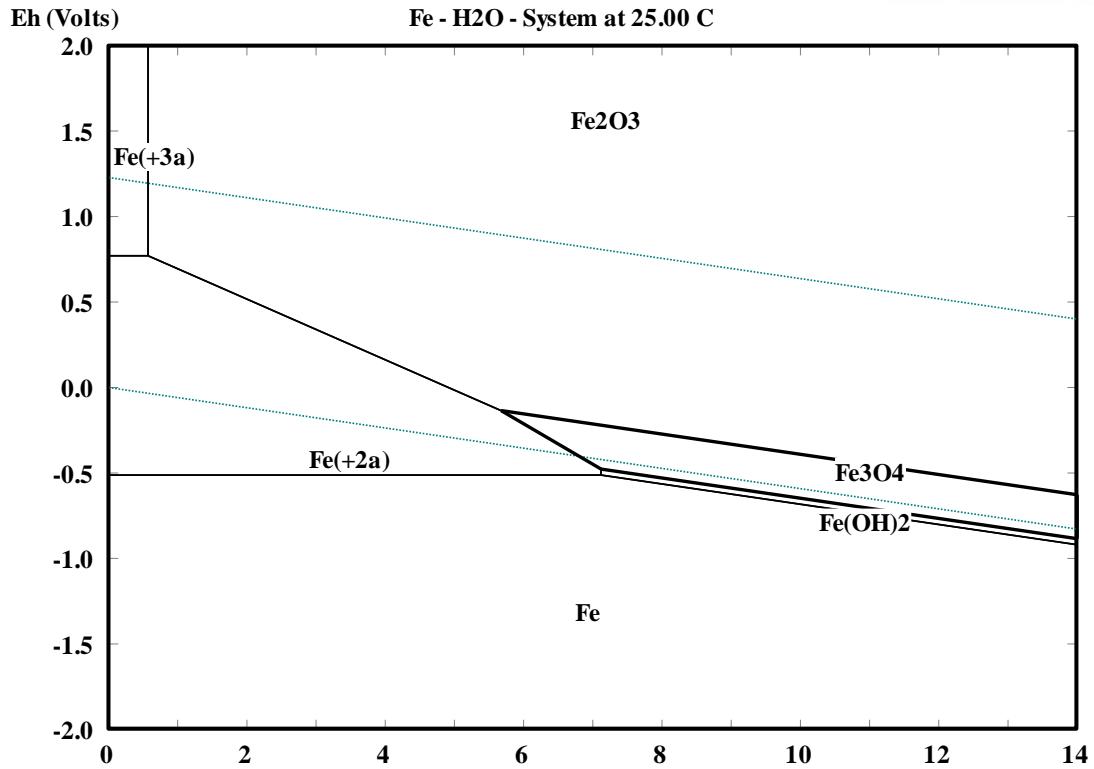
Fe - H2O - System at 150.00 C
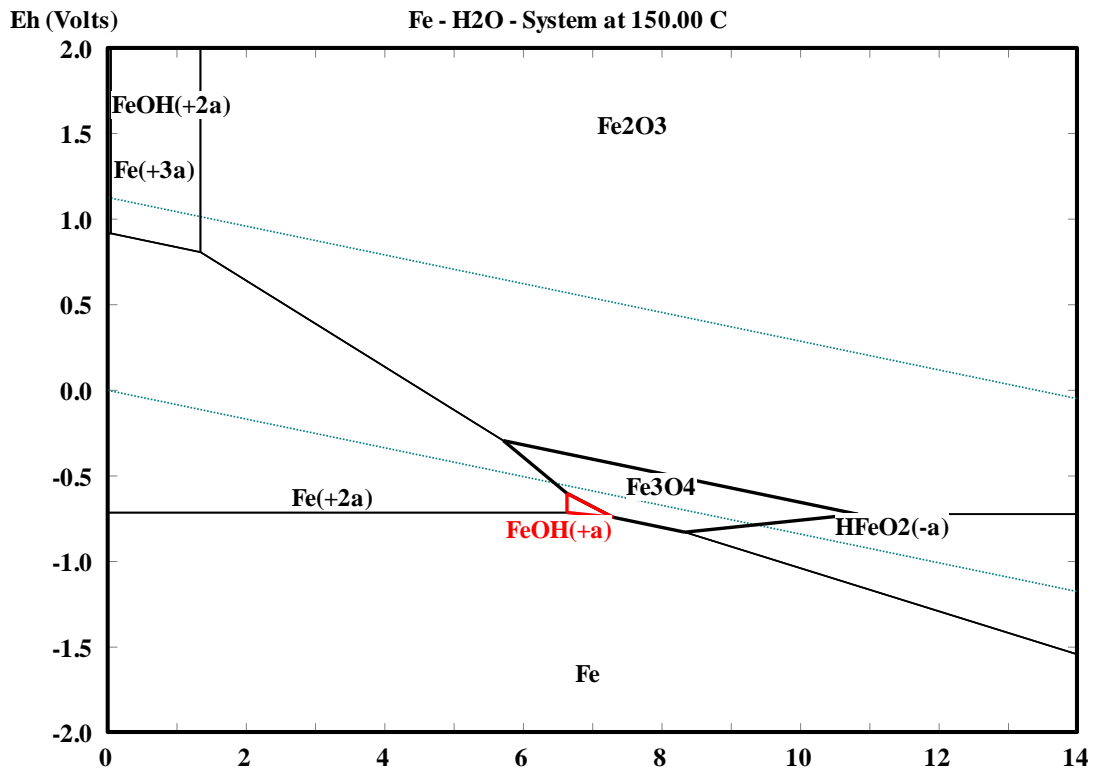
Fig. 2.2 Fe Pourbaix diagram at 150 °C
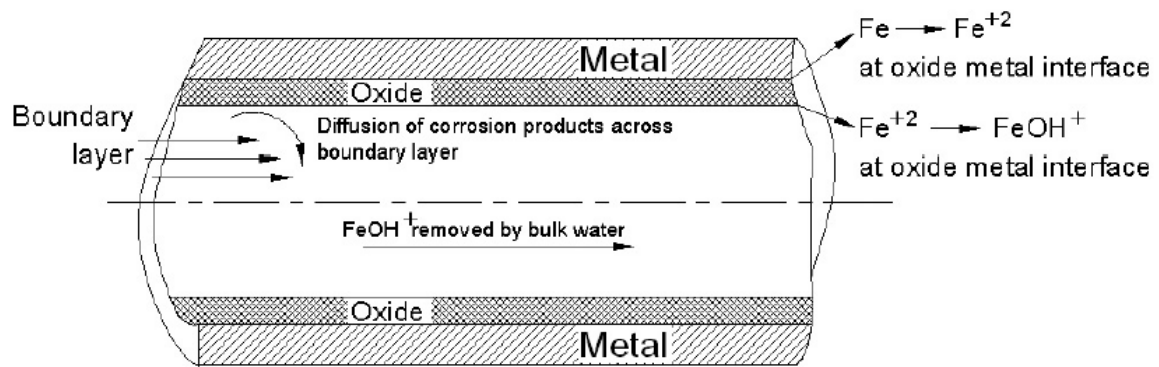
Fig. 2.3 Schematic of the Fe_3O_4 dissolution of FAC [8]
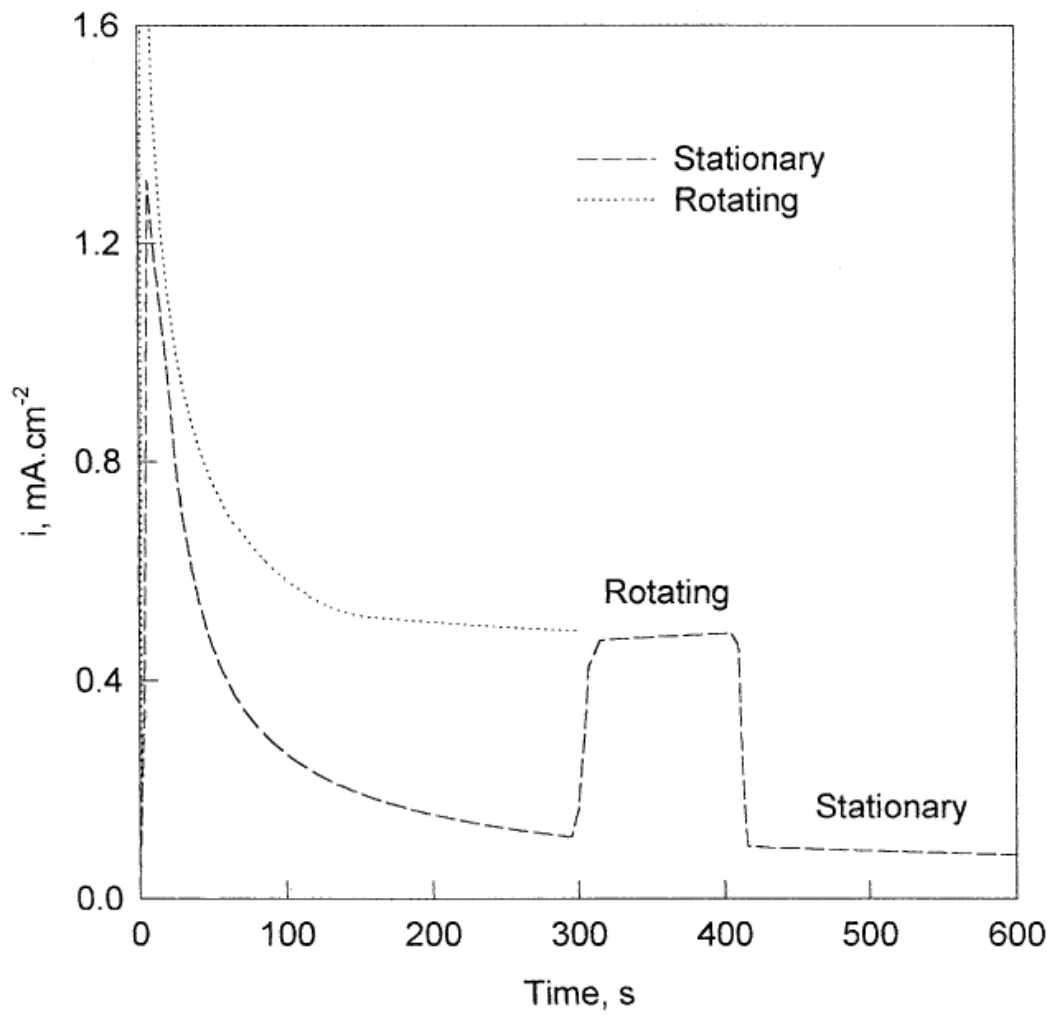
Fig. 2.4 The effect of rotation at -0.8 V at 125 °C [13]
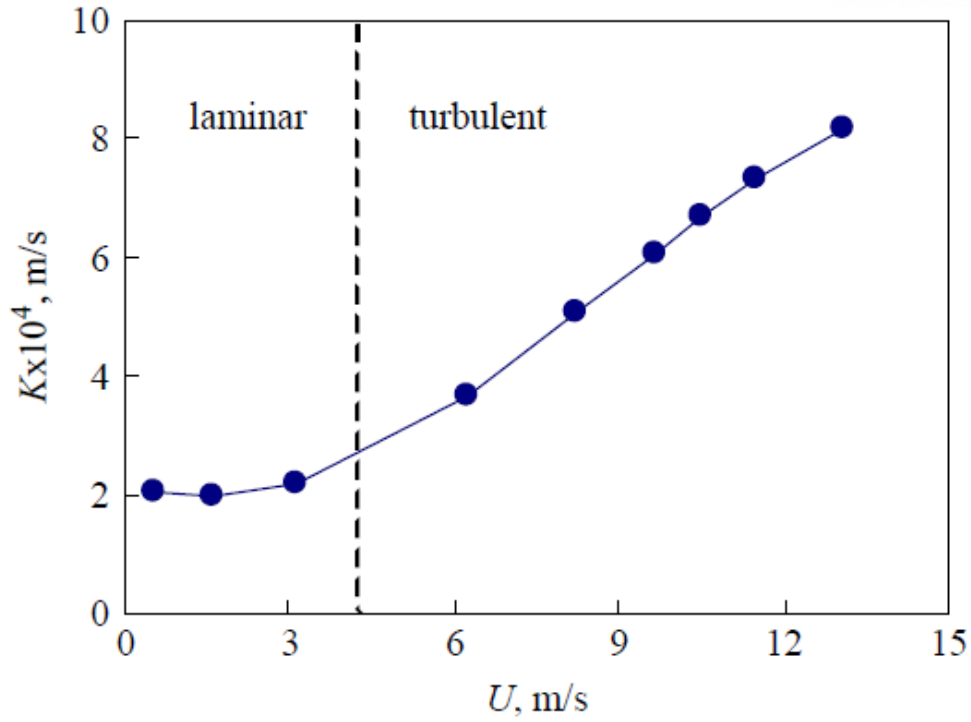
Fig. 2.5 The effect of velocity to mass transfer coefficient [12]
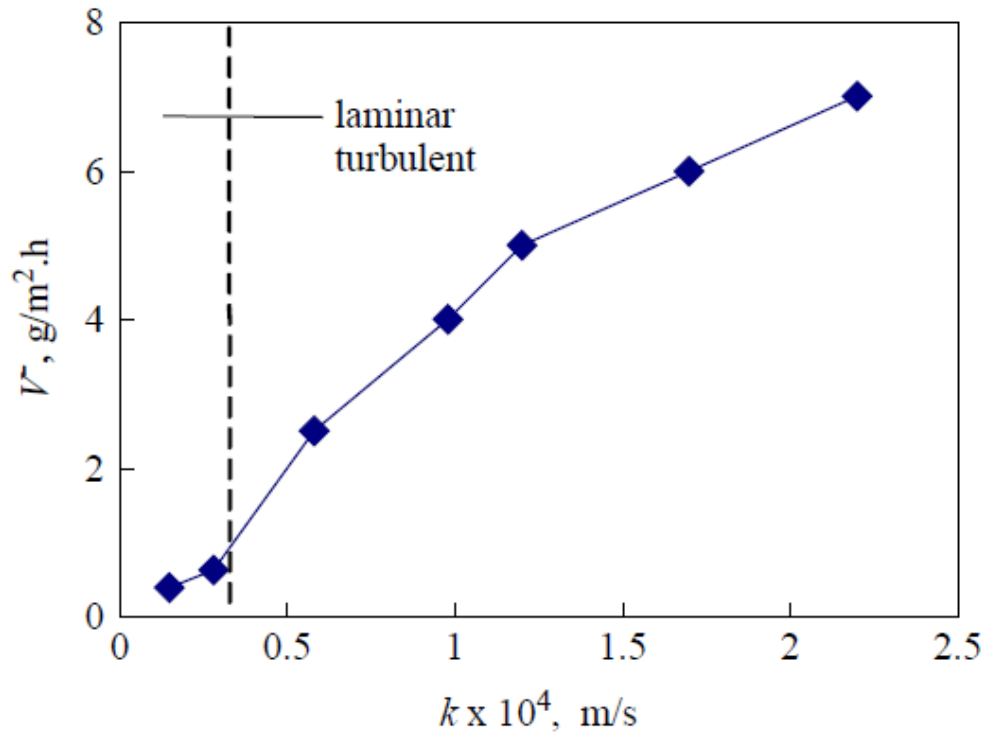
Fig. 2.6 The effect of mass transfer coefficient to metal loss [12]
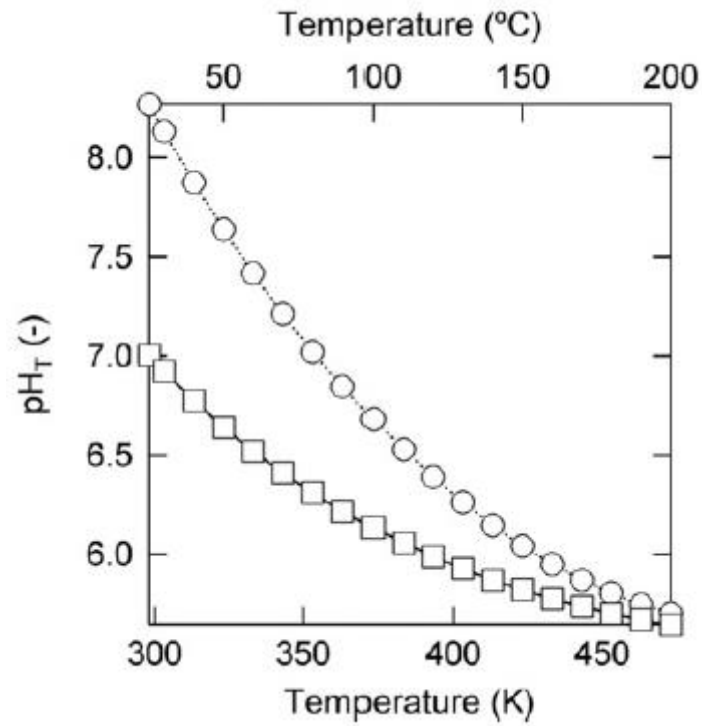
Fig. 2.7 Effect of temperature on pHT in neutral solution [14]
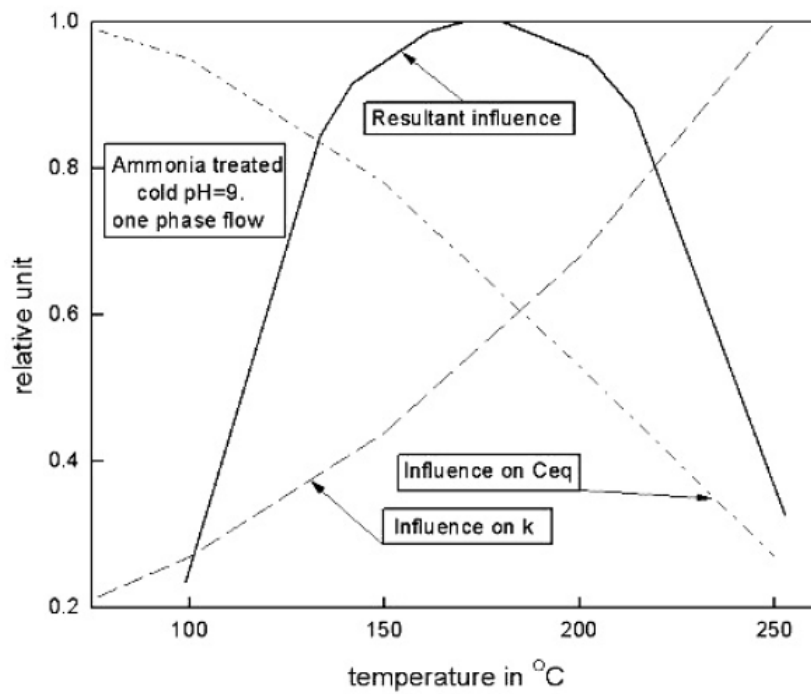
Fig. 2.8 Effect of temperature on MTC and solubility of iron [15]
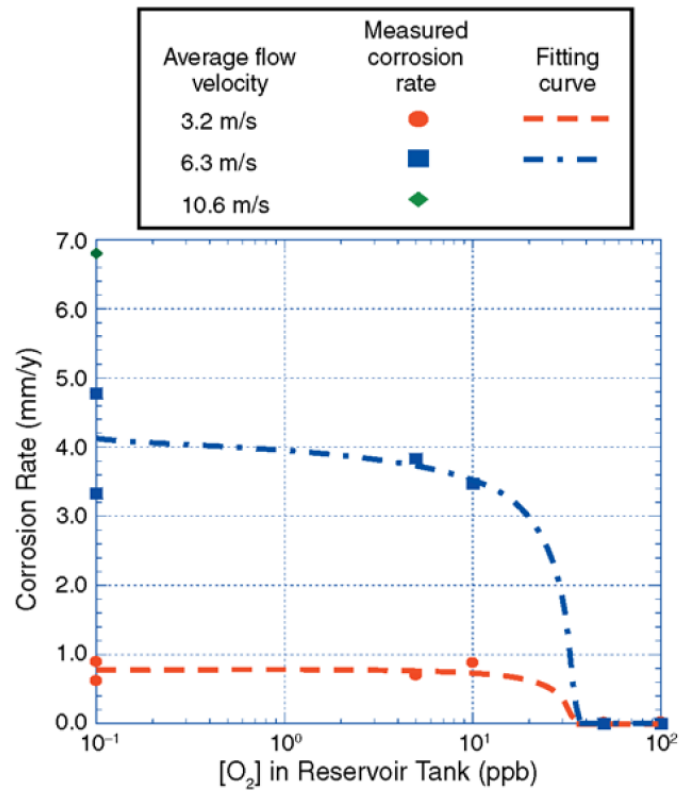
Fig. 2.9 Effect of oxygen in water to corrosion rate [16]
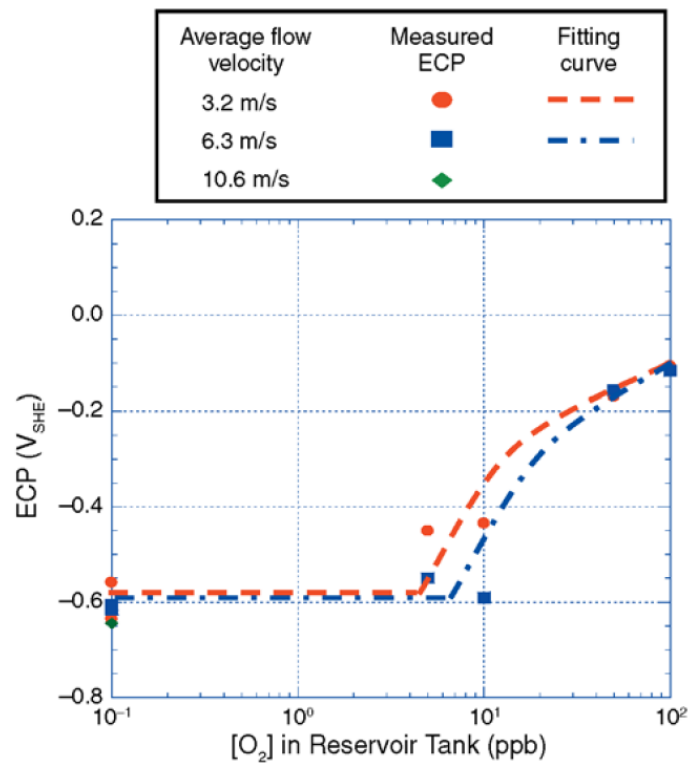
Fig. 2.10 Effect of oxygen in water to ECP [16]

25
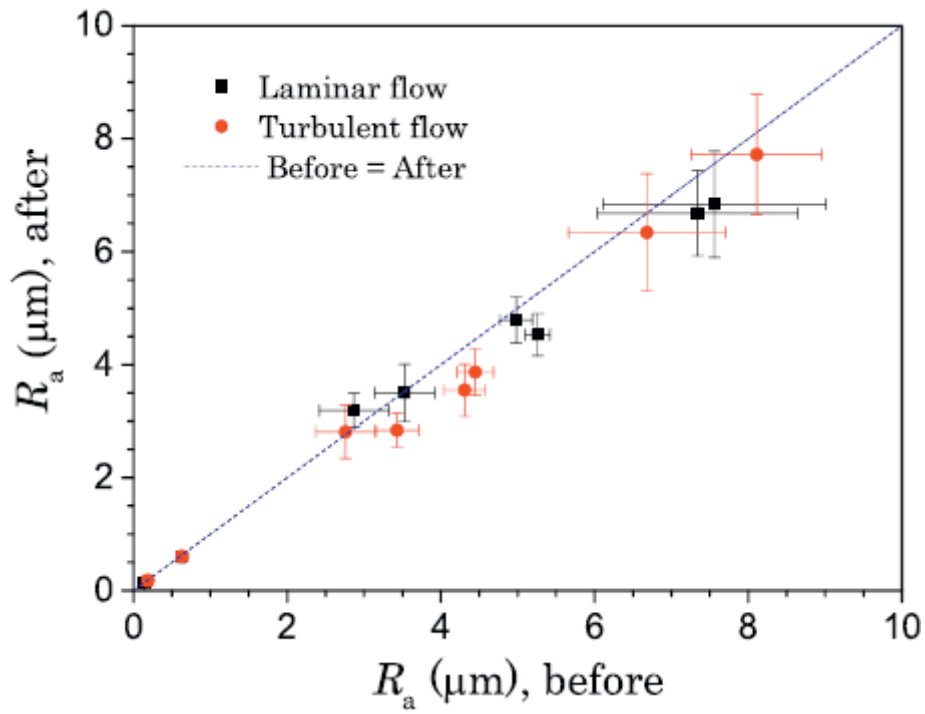
Fig. 2.11 Change of surface roughness under laminar and turbulent flowing conditions [17]
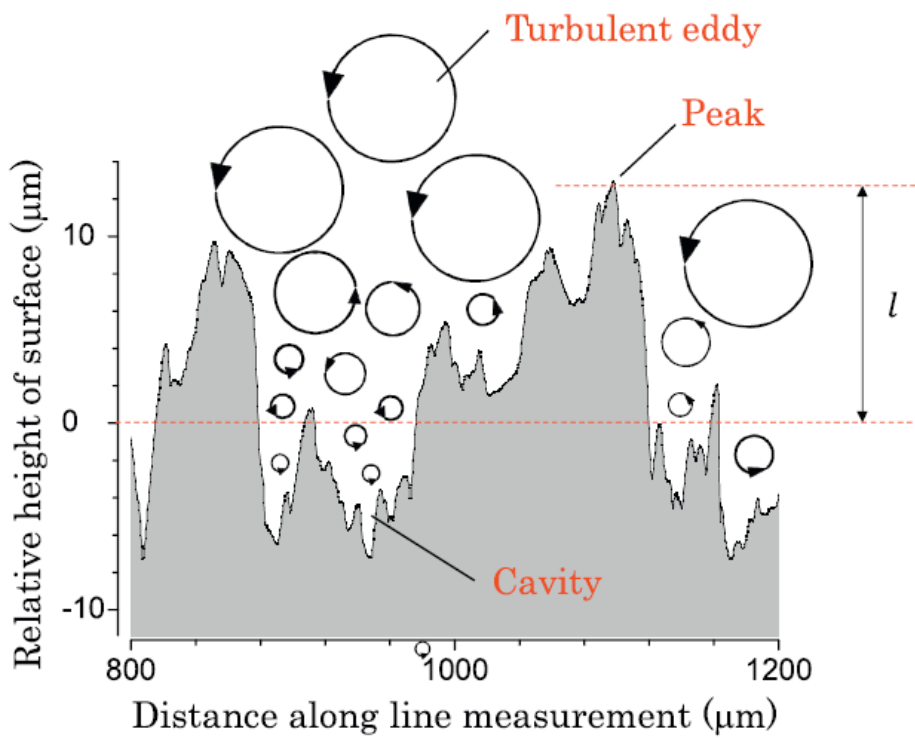
Fig. 2.12 Turbulent eddy formation by rough surface [17]
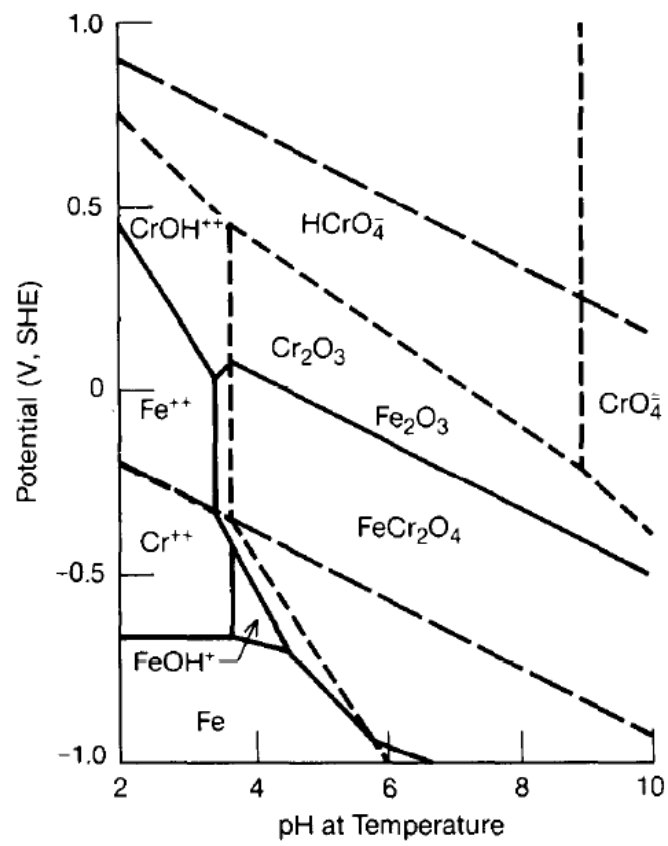
Fig. 2.13 Pourbaix diagram of Fe-Cr-H_2O system at 200 °C [17]
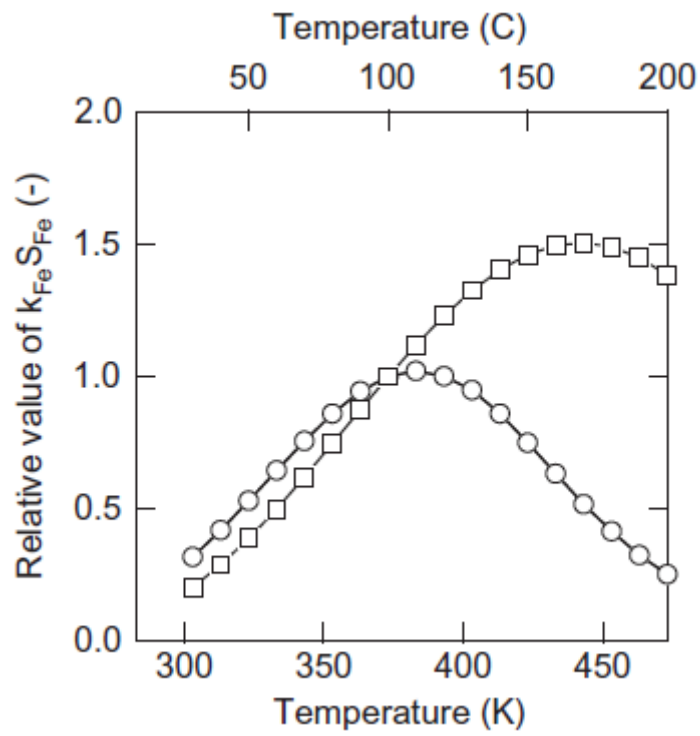
Fig. 2.14 Iron concentration at the solution/oxide interface at various temperature and pH [14]

III. Rationale

3.1 Methods to estimate corrosion rate

3.1.1 Weight measurement

Measurements of difference between weight before and after experiments obtain quantitatively data identifying the extent of the corrosion practically. Experimental time and money should be spent in order to obtain accurate and reliable data. However, the experimentally obtained value after long periods of time can be considered as a reliable data when applied to the industrial field.

3.1.2 Potentiodynamic polarization experiments

The basic process of corrosion situation is electron production or consumption by reaction with solution.

$$Me^{n+} + ne^- \rightarrow Me \tag{11}$$

$$nH_2O + ne^- \rightarrow \frac{n}{2}H_2 + nOH^- \tag{12}$$

Therefore, it can be represented by circuit which is current flows. In potentiodynamic polarization experiments, working electrode (WE) where metal degradation occurs and counter electrode (CE) that offers opposite reaction to WE is needed. Electron emission by corrosion between WE and CE generates flow of current. As a results, high current density indicates WE reaction with solution is increased and corrosion of WE is more severe than before. In experiments, the voltage difference between CE and RE is not possible to measure by absolute potential so reference electrode (RE) is used. The relationship between current density and potential can be measured by differences of relative values between RE and WE [2, 18].

In addition, corrosion rate can be calculated by current density by using Faraday's law. Therefore, measurements of corrosion properties can be carried out qualitatively without the actual corrosion experiment. The equation of corrosion rate is following

$$r = \frac{m}{tA} = \frac{ia}{nF} \qquad (13)$$

Moreover, potentiodynamic polarization experiments need less time because it artificially creates oxidizing and reducing environments by potential difference between WE and CE. Therefore, estimation of corrosion properties by potentiodynamic polarization experiments is more convenient methods than weight measurements.

3.2 Cold spray coating

Changes properties of secondary water chemistry in order to prevent corrosion or characteristics of the tubing by adding other elements have disadvantages that the former cannot be overall solution for decreases about Fe_3O_4 dissolution and the latter has a weakness about price competitiveness.

Therefore, as a way to improve the rate of corrosion, coating to inner surface of pipe can be one of the methods. Coating the metal with better corrosion resistance than Fe, main elements that is used at secondary system, is more convenient methods than the approaches mentioned above because of time and cost. For examples, sol-gel coating and plating which is divided electro and electroless plating have been widely used. However, these coating techniques have a weakness that very thin layer can be obtained. Therefore, for achieving a thick layer to resist to corrosive environment, convenience and compatibility, the thermal spray coating is one of the methods to decrease corrosion rate. For examples, high velocity oxy fuel (HVOF), detonation gun (D-gun), flame spray, arc spray and plasma spray are widely used [19, 20]. Characteristic of the thermal spray coating is in Table 3.1.

Although being similar with the thermal spray, cold spray coating operated by lower temperature than other thermal spray coating was developed first from Russia at 1980s [19]. In cold spray coating, heating energy is used to increase temperature and kinetic energy of carrier gas which moves powder from spray nozzle to substrates surface instead of increasing powder temperature. Therefore, powder ejected from nozzle by carrier gas such as compressed air, N_2 or He collides with substrate. The energy generated at this moment is converted to energy for plastic deformation of powder. Finally, these plastic deformation properties have powder to bond to the substrates [21, 22]. Therefore, the biggest difference between cold spray coating and the other thermal spray coating is usage of heating energy. A former uses energy to increase velocity of carrier gas for kinetic energy and a latter uses energy to melt powder. Illustration of cold spray coating machine is summarized at Fig. 3.2.

Minimum of velocity value for adhesion to surface at substrates during collision is critical velocity and these value is different by mechanical properties, melting temperature, initial temperature of particle, temperature of carrier gas and the working environment such as distance between nozzle and substrates and diameter of nozzle. Ductile material which means plastic deformation occurs easily has low critical velocity. Therefore, it is possible to coat at low temperature. For examples, nickel (Ni), cobalt (Co), aluminum (Al) or copper (Cu) are one of the materials used at cold spray coating [19, 20, 22], 23].

One of the advantage of low operating temperature at cold spray coating is residual stress after coating. Comparing with cold spray, for example, HVOF needs at least 3000K in operation [24, 25]. After operation, coated specimens are cooled under the external environment which is room temperature. High temperature gradient between coated specimens and the external environment creates residual stress at coating layer [19, 20]. On the other hands, cold spray coating operates at relatively low temperature below 1000K so thermal stress to substrates during operation and residual stress at coating layer after coating are decreased [22].

In thermal spray coating, a number of studies indicates that other chemical compounds, unexpected compounds such as decarburized carbide or oxide, are observed at coating layer [26-28]. It is caused by high temperature of thermal spray coating. When melted powder is ejected from the nozzle, these powder can react with outside air and be oxidized. Moreover, in case of carbide, high temperature activates decarburization so unexpected mechanical properties or corrosion properties are investigated [28]. However, low temperature of cold spray coating cannot serve enough energy in order to oxidation or decarburization. Therefore, powder used in spray has less deformation like an oxidation and decarburization [29-31].

3.3 Properties of tungsten carbide and nickel

3.3.1 Tungsten carbide

As a kind of the carbide, tungsten carbide (WC) has better wear resistance than W, W_2C or WC_{1-x}. Comparison of friction coefficient between WC and the other tungsten compounds at Fig. 3.5 indicates WC has low friction coefficient [32]. Moreover, high hardness and wear resistance of WC can be applied to tools for cutting [33]. For example, the Mohs hardness of WC is 9.8 which means WC has similar value with diamonds.

In addition, high corrosion resistance to acidic condition is applied to powder metallurgy by sintering [34]. For examples, sintered body produced by WC is often used at automotive industry such as wheel

that contact with the acidified or neutral environment [35, 36].

Pseudo Pourbaix diagram by using chronopotentiometric titrations (CP) at Fig. 3.6 shows that WC has better corrosion resistance than W. Although $0.01 mA/cm^2$ is assumed as small amount of current density that oxidation product is not dissolved to water, large passivation region of WC indicates passive layer of WC is stable at corrosive environments [37].

WC reaction with water at various pH forms WO_3 by the following equation [38].

$$WC + 5H_2O \rightarrow WO_3 + CO_2 + 10H^+ + 10e^- \tag{14}$$

$$WC + 4H_2O \rightarrow WO_2(s) + CO_2 + 8H^+ + 8e^- \tag{15}$$

$$WC + 3H_2O \rightarrow WO_3(s) + CH_4 + H_2 \tag{16}$$

$$WO_2(s) + H_2O \rightarrow WO_3(s) + 2H^+ + 2e^- \tag{17}$$
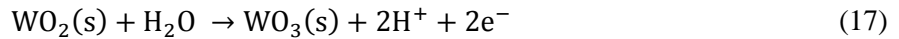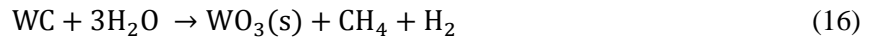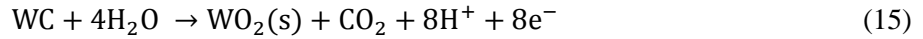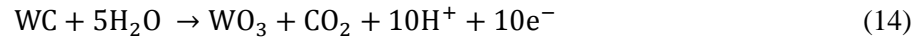
The difference of passivity between acidic and alkaline condition is caused by the oxide dissolutions at water and these dissolutions occur by the following reaction [38].

$$WO_3 + H_2O \rightarrow WO_4^{2-} + 2H^+ \tag{18}$$

$$WO_3(s) + OH^- \rightarrow WO_4^{2-}(aq) + H^+ \tag{19}$$

$$WO_2(s) + 2H_2O \rightarrow WO_4^{2-}(aq) + 4H^+ + 2e^- \tag{20}$$
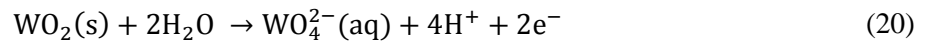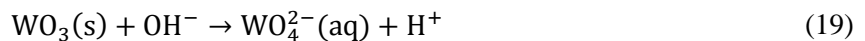
In equation (19), WO_3 reacts with OH$^-$ and dissolves to the water it means WO_3 are not stable at high pH solution. Moreover, in high pH water, WC can be dissolved directly by forming tungsten ion. These reaction is explained by equation (21). Therefore, passivation region is narrower at high pH condition than low pH condition.

$$WC + 14OH^- \rightarrow WO_4^{2-} + CO_3^{2-} + 7H_2O + 10e^- \tag{21}$$
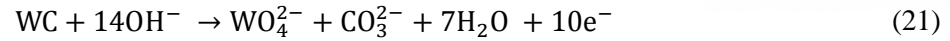
During cold spray coating process, WC has high melting temperature,3073K, and poor plastic deformation properties so these properties is obstacle to obtain good efficiency. Moreover, surface oxidation and dissolution at alkaline solution is more severe than that at acidic condition. In order to eliminate the limitations, carbide with binder metal which has low melting temperature such as Co or Ni was developed. It has been widely used at cold spray coating with carrier gas such as N_2 or He.

For example, Co, Ni, Fe or Cu is a material which is a binder metal and WC with binder metal is named as cemented carbide or hard metal.

3.3.2 Nickel

Corrosion behavior of Ni investigated by Pourbaix diagram and literature study indicate reduction potential at alkaline solution is lower than WC. Although Pourbaix diagram at Fig. 3.7 and schematics at Fig. 3.8 mean transformation from $Ni(OH)_2$ to oxide of Ni occurs at severe condition [2], corrosion product at experiments is different with Pourbaix diagram [39-41].

When WC without Ni is coated to carbon steel, weakness of corrosion resistance to alkaline solution influences on WC and WO_3 dissolution. For reducing dissolution of WC, coating with binder metal such as Ni is useful methods in order to create composite compound.
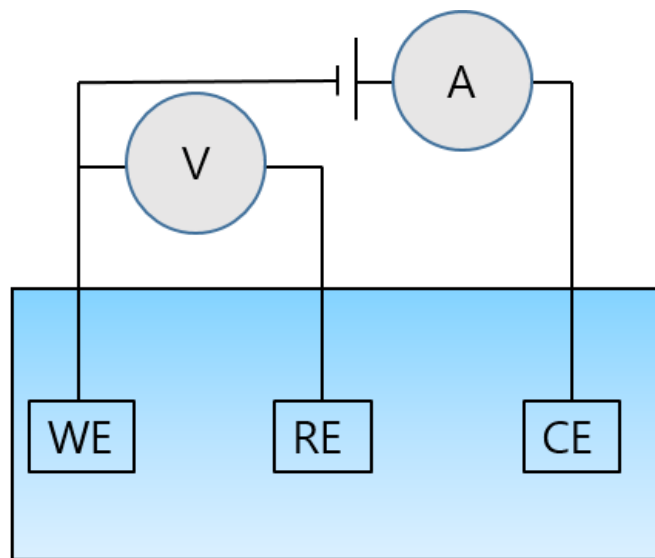
Fig. 3.1 Schematics of three electrode system

Table. 3.1 Characteristics of the thermal spray coating

Thermal spray	Temperature(K)	Velocity(m/s^2)	Porosity(%)
Flame spray	1500~3000	150~350	10~20
Plasma spray	2500~16500	400~650	1~10
Arc spray	4000~6000	200~450	5~20
Detonation gun spray	2500~4500	700~900	~5
High velocity oxy fuel spray	1500~3500	500~800	~5
Cold spray	400~1000	300~1500	~5
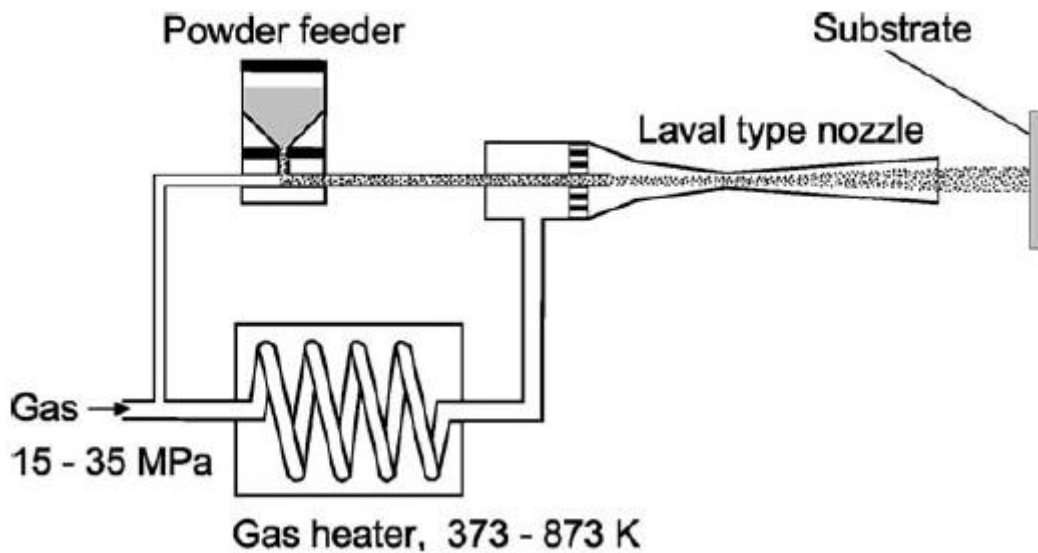
Fig. 3.2 Illustration of cold spray coating machine [21]
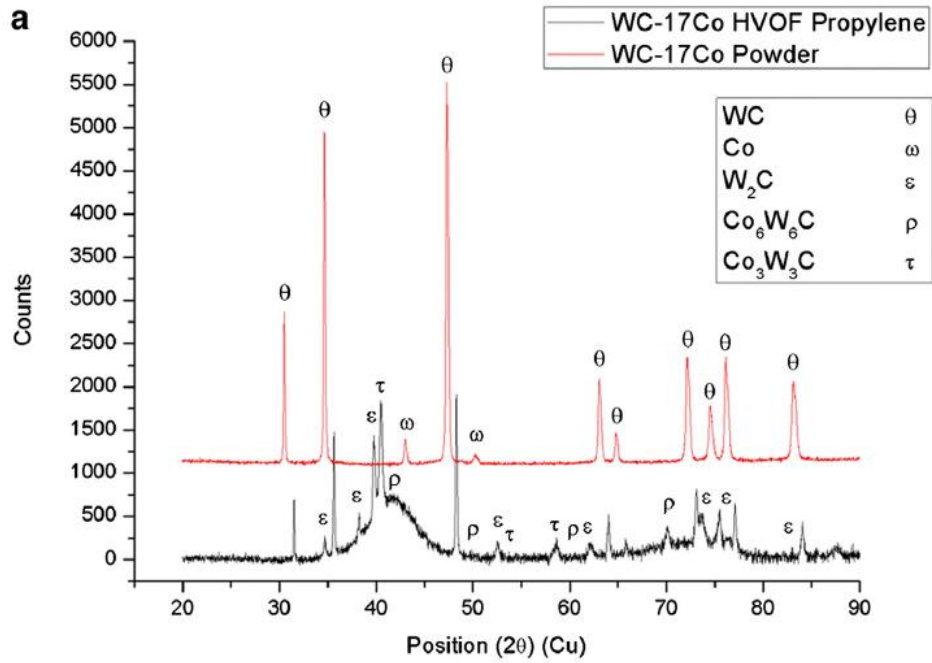
Fig. 3.3 XRD analysis of WC-Co powder and WC-Co HVOF coating [29]
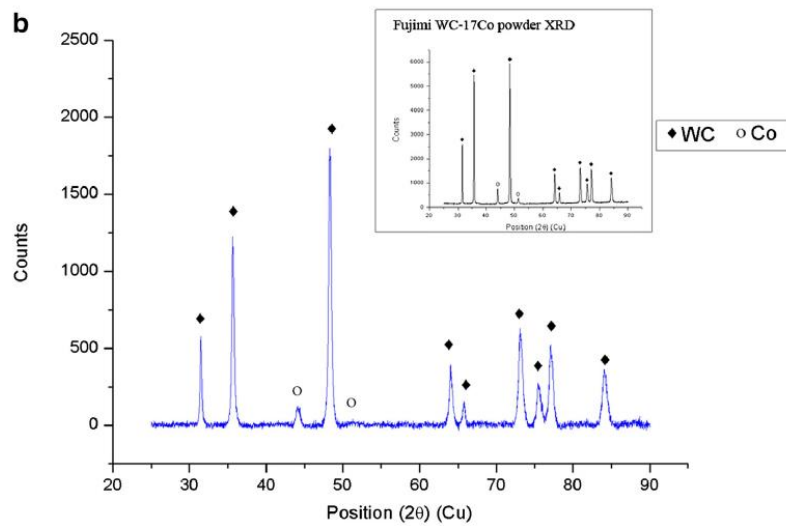
Fig. 3.4 XRD analysis of WC-Co powder and WC-Co cold spray coating [29]
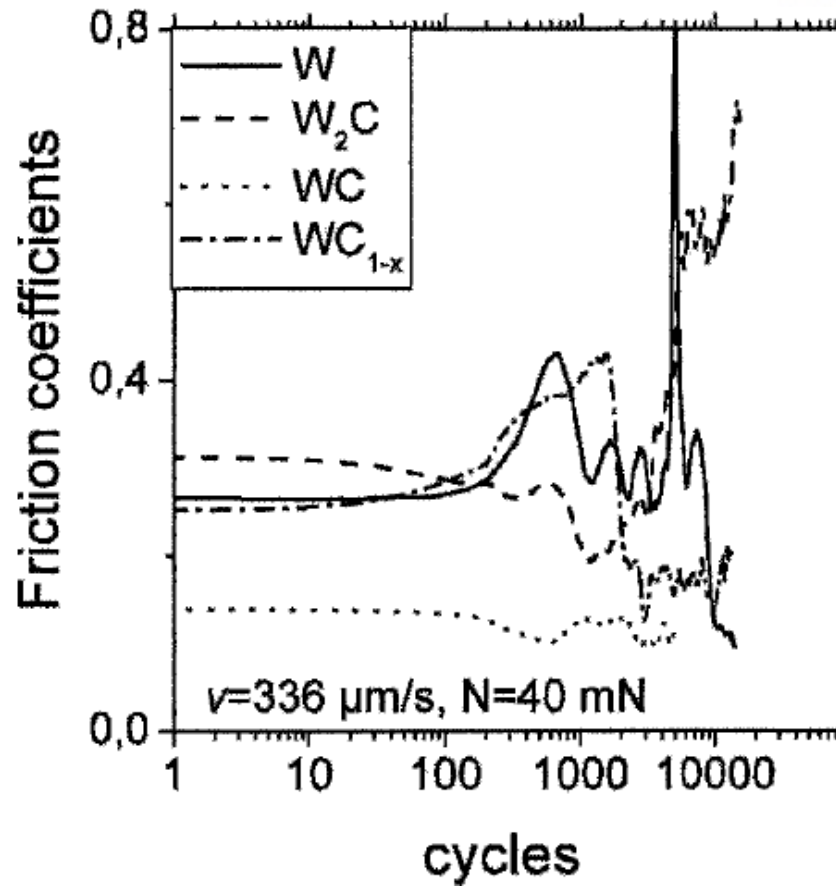
Fig. 3.5 Friction coefficient of WC compared with other tungsten compounds [32]
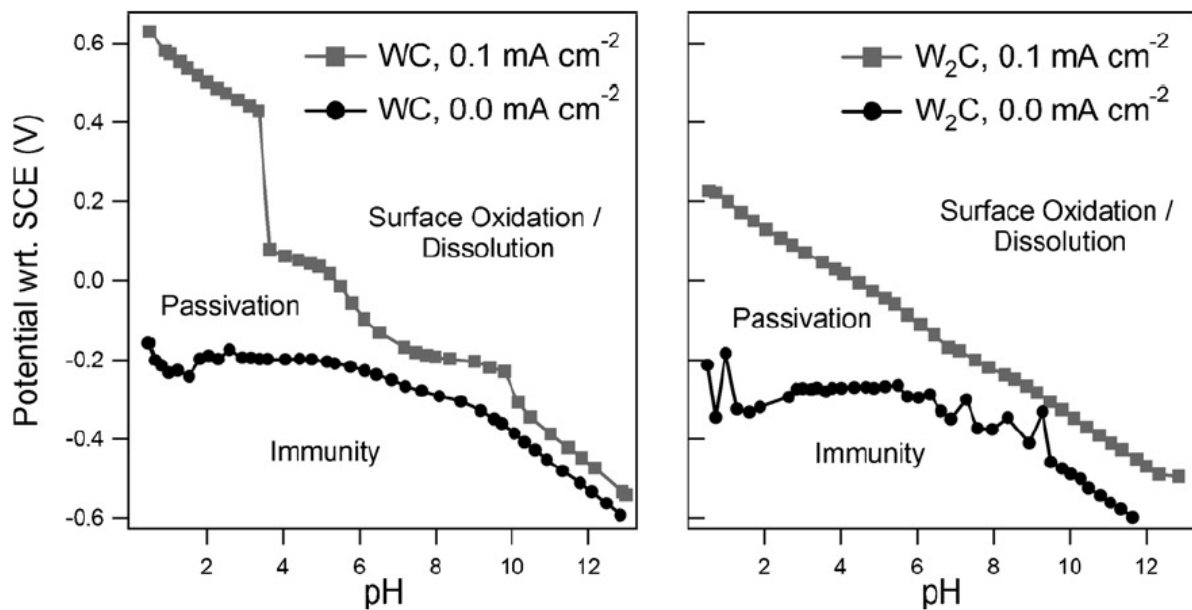
Fig. 3.6 Comparison of CP titration experiments for stability mapping on WC, W_2C [37]
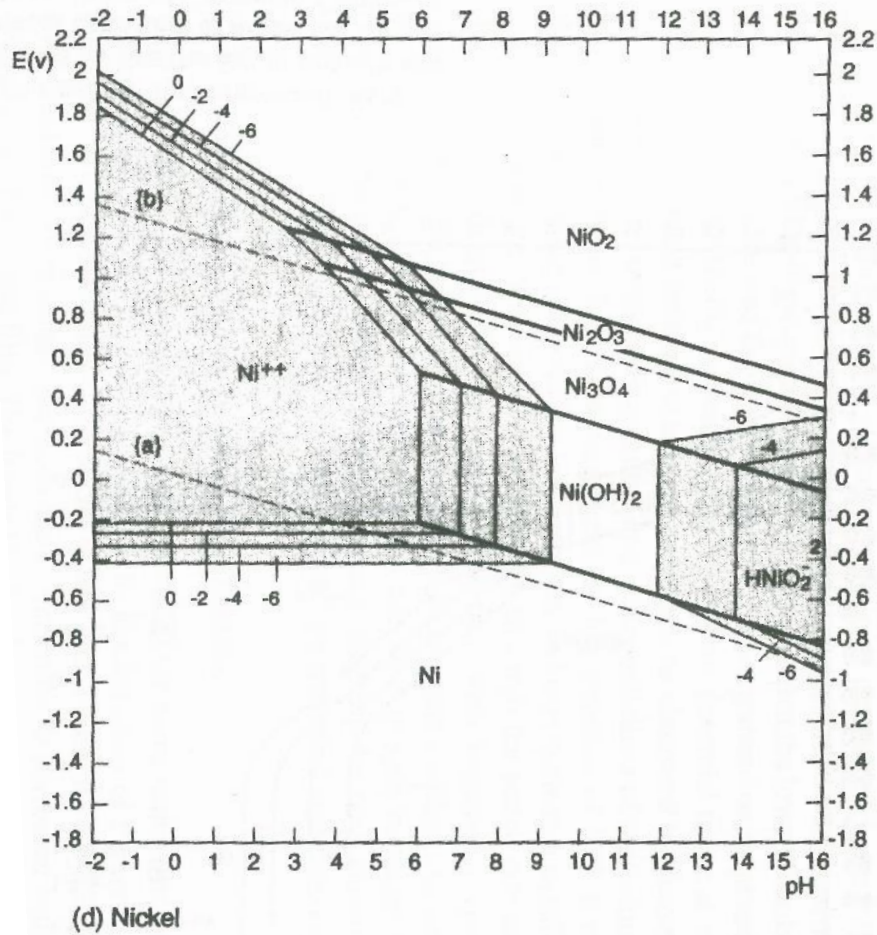
Fig. 3.7 Nickel Pourbaix diagram at 25 °C [39]
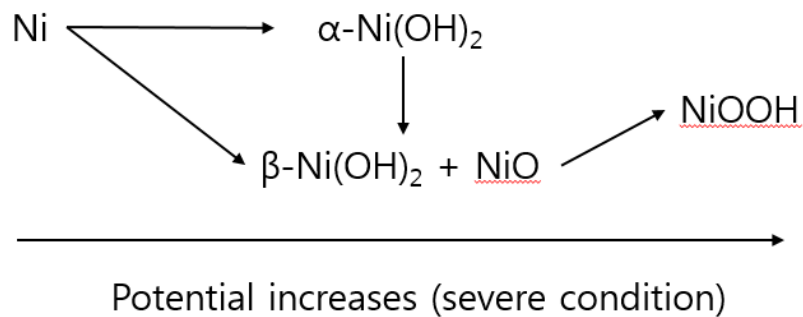
Fig. 3.8 General scheme presenting relationships Ni oxidation at alkaline media [41]

IV. Experimental

4.1 Specimen preparation

4.1.1 Powder production

4.1.1.1 WC-10Ni spray dried methods

Small size of power is an advantage for coating in order to achieve uniform coating but coating efficiency is dramatically decreased because particles spreads out from a nozzle and slip down at outlet of nozzle. However, small size of WC is better corrosion resistance at alkaline solution than micron size [42, 43]. Therefore, particle including nano WC (200 nm-400 nm) needs to be larger without WC agglomeration.

As a results, WC-10 wt.%Ni powder (5~30 μm) is made by spray dried methods in order to promote coating efficiency without WC agglomeration from Buffalo Tungsten Inc. (BTI). The image of WC-10Ni are shown at Fig. 4.1

4.1.1.2 Electrolysis production

WC-10Ni powder is hollow particle inside and these shape influences on weight of particle. Light weight of WC-10Ni decreases kinetic energy so plastic deformation of powder is difficult. Moreover, the ratio of WC in powder raises critical velocity so it is possible to coat only by using carrier gas such as N_2, He. Although N_2 or He helps particle to achieve higher velocity over the critical velocity than compressed air, it spends lots of money and does not have economic benefits compared to P22, alternatives of carbon steel.

Consequently, ductile and not hollow particle is needed for coating efficiency. For producing these powder acting like a glue with inexpensive costs, electrolysis methods are chosen. Ductile material is selected as Ni and these powder is produced at Rus Sonic Technology, Inc. (RSTI). The SEM image of Ni is shown Fig. 4.1

4.1.2 Cold spray coating

Maintenance of coating efficiency about 40% is well achieved by using relatively low temperature and pressure because Ni is ductile material and has low melting temperature. However, Ni with WC-10Ni powder needs high pressure and temperature when compressed air is used as carrier gas. Therefore, after considering D. Lioma et al., [44] and the performance of cold spray coating machine at RSTI, coating parameter is chosen. Cold spray coating is carried out at RSTI to carbon steel (90mm*60mm * 5mm) and cut to small plate specimens (20mm * 20mm * 5mm) by discharge machining at UNIST. After coating, scanning electron microscope (SEM) and Energy-dispersive X-ray spectroscopy (EDS) analysis is carried out for coating properties.

4.2. Experimental procedures

4.2.1 Potentiodynamic polarization experiments at room temperature

Before FAC simulation experiments at high temperature, corrosion resistance in pH 9.3 ETA solution at room temperature was measured by potentiodynamic polarization experiments. Hg/HgO reference electrode (0.098 V vs NHE) and Pt as counter electrode are used. Before experiments, carbon steel and P22 are polished by 320, 400, 600 and 800 grit SiC paper and cleaned by ultrasonic washer with acetone, ethanol and DI water each for 2 minutes for eliminating oxide layer at substrates. Working electrodes are carbon steel, WC-10Ni + 20Ni, WC-10Ni + 25Ni, WC-10Ni + 30Ni coating and P22.

4.2.2 FAC simulation experiments and measurements of weight change

Fig. 4.3 is schematics of FAC simulation experiments loop and image of specimen holder. Coated specimens, carbon steel and P22 are held at specimen holder in autoclave and rotated by magnedrive at a speed of 1100 rpm for simulating turbulent condition. The condition of water chemistry is summarized at Table 4.6 and chosen because corrosion of carbon steel at pH 9.3 solution is maximized at these condition. Although currently operated nuclear power plant in Korea raises pH to 9.5, difference of pH at high temperature is smaller than that of pH at room temperature which is presented Fig. 2.7. Moreover low pH accelerates corrosion of specimens so experiments carried out at pH 9.3. After 2 weeks and 4 weeks FAC experiments, weight change is measured. To investigate the characteristics of the coatings

after corrosion experiments, SEM, EDS and X-ray photoelectron spectroscopy (XPS) analysis is carried out.
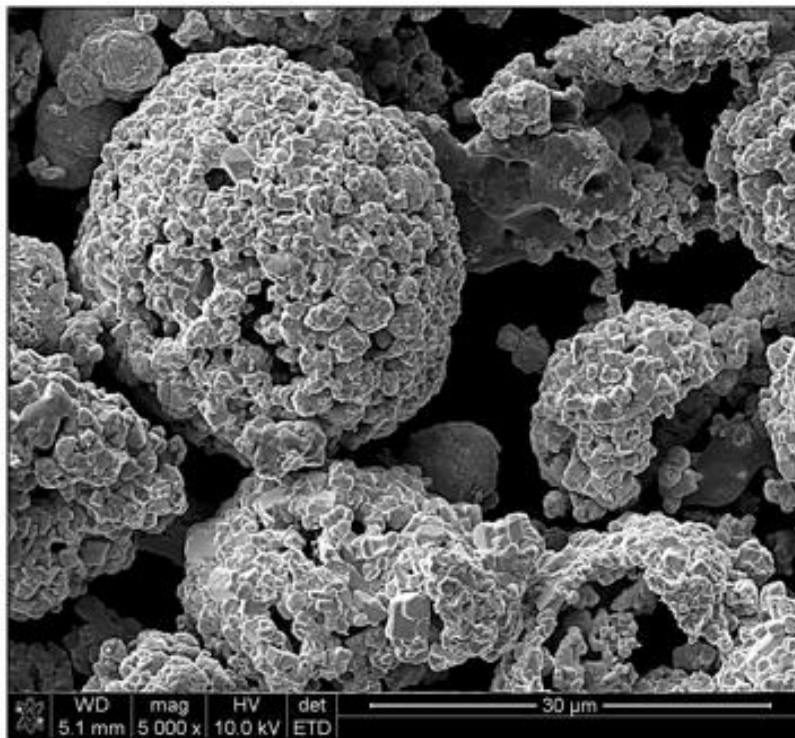
Fig. 4.1 SEM image of WC-10Ni powder

Table. 4.1 Chemical composition of WC-10Ni powder

Element	wt.%	at.%
Ni	8	16
W	89	57
C	3	27
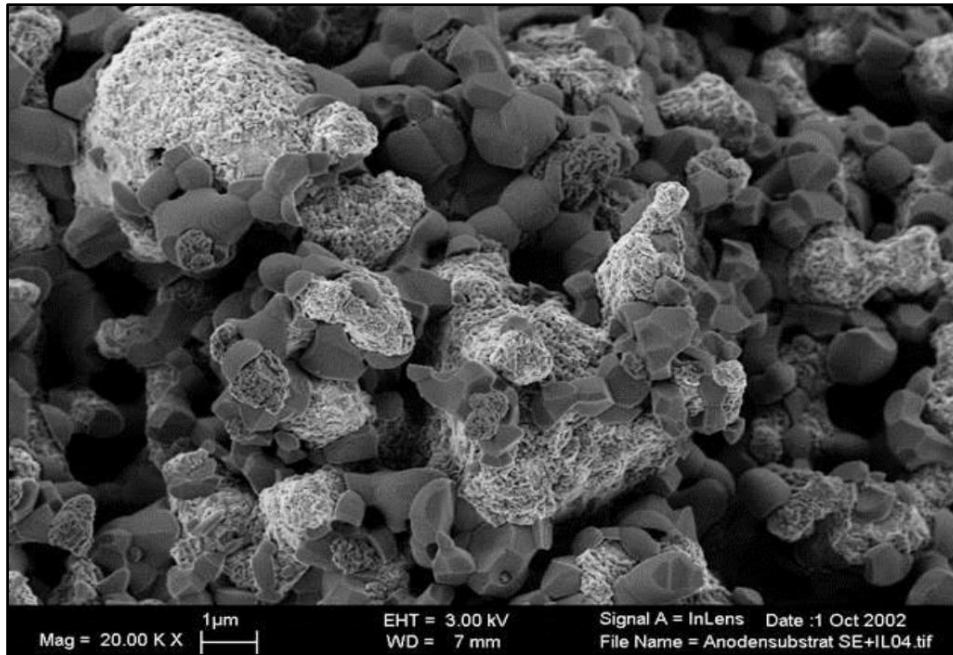
Fig. 4.2 SEM image of Ni powder

Table. 4.2 Chemical composition of Ni powder

Element	wt.%	at.%
Ni	100	100

Table. 4.3 Coating parameter

Pressure	9 bar
Temperature	600 °C
SOD	15 mm
Types of coating	WC-10wt%Ni + 20wt%Ni, +25wt%Ni, and +30wt%Ni

Table. 4.4 Chemical composition of SA 516 Gr.60

Element	C	Si	Mn	P	S	Cu	Ni	Cr	Fe
wt.%	0.13	0.201	0.714	0.0141	0.0041	0.006	0.01	0.006	Balanced

Table. 4.5 Chemical composition of SA 335 Gr. P22

Element	C	Si	Mn	P	S	Cr	Mo	Fe
wt.%	0.13	0.24	0.43	0.011	0.004	2.12	0.96	Balanced
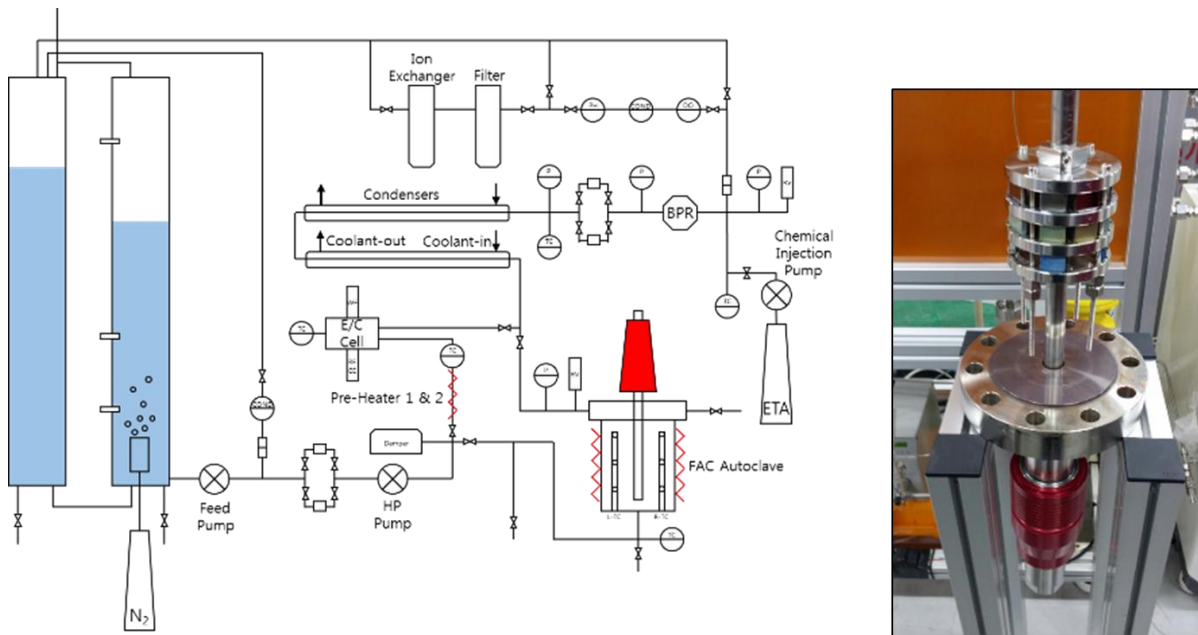
Fig. 4.3 Schematics of FAC simulation experiments loop and image of specimen holder

Table. 4.6 Experimental condition of FAC simulation experiments

Solution	pH 9.3 ETA solution (at room temperature)
Temperature	150 ℃
Simulation time	2weeks and 4weeks
Pressure	70 bar
DO	0 ppb
Specimens	WC-10Ni + 20Ni (4ea) WC-10Ni + 25Ni (4ea) WC-10Ni + 30Ni (4ea) Carbon steel (4ea) P22 (4ea)

V. Results

5.1 Surface and cross-section observation before experiments

Pores at coated surface are observed by SEM and these defects are seen at all of coated area. Although surface is smooth and small porosity are observed after plating coating [45], results of cold spray coating at Fig. 5.1 show surface roughness is larger than plating coating. All of coatings had pore being larger than 10 microns and these pore can be an activation site during corrosion test.

In Fig. 5.2, chemical composition of coating at surface is investigated but atomic and weight ratio are not accurate in case of carbon. Therefore, EDS data analysis only shows that carbon exists in coating. Therefore, formation of the other unexpected composition such as W_2C or W is not observed exactly by EDS analysis. However, oxygen is not detected so other oxide product does not exist in coating.

Because coating is carried out with addition different Ni contents to WC-10Ni, weight ratio calculated mathematically is 25 %, 28 % and 31 % in coating. However, chemical composition of Ni at coating is higher than these values. 54 %, 62 % and 72 % of Ni is measured at 20Ni, 25Ni and 30Ni coating. On the other hands, the chemical composition of W was smaller than expected ratio which is 45 %, 35 % and 25 %. Therefore, increasing of Ni contents at coating process results in raising Ni contents and decreasing W contents of surface of coating. Poor plastic deformation properties of WC decreases ratio of W and ductile properties of Ni increase ratio of Ni during cold spray coating process.

Figs. 5.3 ~ 5.5 show cross-section of coating. Thickness of coating is about between 200 microns and 300 microns. Thermal spray coating has non-uniformity of thickness so it need to be polished for uniform coating. However thick coating layer indicates plastic deformation of Ni and increase of thickness are successfully progressed. An upper section of cross-section indicates that uneven surfaces is achieved after coating and these properties are disadvantage of thermal spray. As with the surface, pores in layer are observed but these pores are located at WC-10Ni particle. Despite using nano WC particle, nano particle is agglomerated after coating process so size of nano particle was larger than micron. On the other hands, coated site distributed Ni have thick and dense layer.

Chemical composition of cross-section is carried out at all section of coating and summed. Unlike the chemical composition at the surface, the ratio of W is measured respectively high and the weight percent of Ni at cross-section is smaller than that at surface. As with the surface, existence of carbon is observed at EDS but accurate ratio cannot be exactly estimated. In case of 20Ni coating, W contents is same with Ni as 45 wt.%. With increasing Ni ratio during coating process, Ni contents are increased and W contents are decreased. Fig. 5.6 shows comparison of chemical composition of cross-section graphically.

5.2 Potentiodynamic polarization experiments

20Ni coating has lower corrosion potential and higher current density than 25Ni coating and 30Ni coating. The value of corrosion current density of 25Ni coating was 50 % of that of 20Ni and 70 % of that of 30Ni. Therefore, 25 wt.% Ni addition during coating process has better corrosion resistance in pH 9.3 ETA solution at room temperature than 20 wt.% Ni and 30 wt.%Ni addition.

Comparing coatings with carbon steel and P22, all of coating have better performance about corrosion in pH 9.3 ETA solution at room temperature than carbon steel but 20Ni and 30Ni coating has higher corrosion current density than P22. However, corrosion current density of 25Ni indicates coating has almost same corrosion properties as compared with P22.

The results of polarization experiments of coating, carbon steel and P22 is illustrated at Figs. 5.7 and 5.8 and Table 5.2.

5.3 Weight change measurements after FAC experiments

Fig. 5.9 shows different corrosion behavior occurs after 2 weeks and 4 weeks FAC simulation test. After 2 weeks, weight gain is observed from 20Ni coating but weight loss is severe with increasing Ni contents. Weight gain from 20Ni coating is about 0.881 mg/cm^2 and weight loss of 25Ni and 30Ni coating is about 0.387 mg/cm^2 at 25Ni coating and 0.862 mg/cm^2 after 2 weeks. Significant weight loss form carbon steel occurs and that value was 3.28 mg/cm^2. P22 has same results with polarization experiments which means reduction of weight is smaller than 30Ni coating and similar with 25Ni coating.

However, weight change of coating after 4 weeks is different from that of coating after 2 weeks. Weight loss from 20Ni occurs after 4 weeks FAC simulation test contrary to 2 weeks results and the difference of weight between 2 weeks and 4 weeks was approximately 3 mg/cm^2. On the other hands, the tendency of weight loss at 25Ni coating after 2 weeks was reversed to the tendency of weight gain and the weight increase was about 1.89 mg/cm^2.

Reduction of weight of P22 is about 0.4 mg/cm^2 after 2 weeks and 0.675 mg/cm^2 after 4 weeks. The value of P22 after 4 weeks is smaller than carbon steel, 20Ni and 30Ni coating.

5.4 Surface and cross-section observation after FAC simulation experiments

Fig. 5.10 and 11 show SEM image of coated surface after 2 weeks and 4 weeks. Significant difference with time between coatings is not observed at surface but coated surface is seemed like erosion by a certain direction. The reason of this phenomenon is flow direction simulated by FAC loop and rotation of magnedrive.

Chemical composition of surface after 2 weeks shows similar tendency with chemical composition of surface before experiments and contents of Ni is increased with increasing ratio of Ni addition during coating process. As a results of FAC simulation experiments, oxygen was detected from EDS analysis and ratio of oxygen was about half of Ni contents at coating and two times of W contents approximately. On the other hands, EDS data from coating after 4 weeks FAC experiments at Fig. 5.13 shows different tendency. W contents is slightly increased and Ni contents is decreased at 25Ni coating.

Because two different powder are mixed and used during coating process, two characteristics are observed after FAC simulation. At a surface after experiments, precipitates in red circle at Fig. 5.14 is observed above Ni and elements of these precipitates are Ni and O. And a small amount of W is observed by EDS. Therefore, these precipitates are oxidation products of Ni. Comparing with blue section and yellow section, WC with Ni region such as blue section has higher Ni contents than yellow section. Moreover, only WC particle without Ni matrix is observed at surface after FAC simulation experiments.

Figs. 5.15 and 16 show cross-section of coating after FAC experiments. However thick oxide layer above micron is not observed and thickness between 2 weeks and 4 weeks is not significantly different. At line EDS analysis, thickness of layer is about below 500 nm. Moreover, rough surface and porosity at the surface influence on corrosion at inside of coating so oxygen is detected inside.

5.5 X-ray photoelectron spectroscopy analysis

5.5.1 X-ray photoelectron spectroscopy data of Ni

The outermost surface is assumed to be damage during discharge machining for usage to XPS analysis. Therefore, XPS data of coating after FAC simulation experiments is compared with as-sprayed specimens after 420s etching. The results after 420s etching are shown in Fig. 5.19. $Ni(OH)_2$ is observed

and other oxidation products of Ni such as NiO and NiOOH are not detected by XPS. The detection of Ni at surface before experiments without NiO or $Ni(OH)_2$ indicates cold spray coating reduces oxidation of powder during coating process.

After 2020s etching, the fraction of $Ni(OH)_2$ is increased with Ni contents because normalized counts of $Ni(OH)_2$ is increased by Ni contents at coating. Compared with 2 weeks specimens, coatings after 4 weeks experiment have sharper and higher peak at $Ni(OH)_2$ region than coatings before experiments. Moreover, the difference of $Ni(OH)_2$ peak between 2 weeks and 4 weeks indicates oxide layer becomes thick and dissolution of coating layer is smaller than oxidation of coating layer.

5.5.2 X-ray photoelectron spectroscopy data of W

On surface of coating, WC and WO_3 coexist and noticeable change of XPS results is observed at 25Ni coating. The ratio of WO_3 is decreased at 4 weeks. The ratio of WC at 25Ni coating is increased after 4 weeks but other coating has not significant change of chemical composition of WC and WO_3. Other oxidized or decarburized products such as W_2C, W or WO_2 is not detected at surface before experiments. Low temperature at cold spray influences on decarburization or oxidation of WC during coating process and reduces powder deformation.

Ratio of WO_3 is increased by experiments time at inside of coating (2020 s etching). The increase of WO_3 at 30Ni coating after 4 weeks comparing with 2 weeks is larger than 20Ni and 25Ni coating. After 2 weeks, oxidation occurs at deep inside (2020 s) of 20Ni and 25Ni coating but noticeable peak of WO_3 is not observed at 30Ni which means oxidation of WC is smaller than other coating.
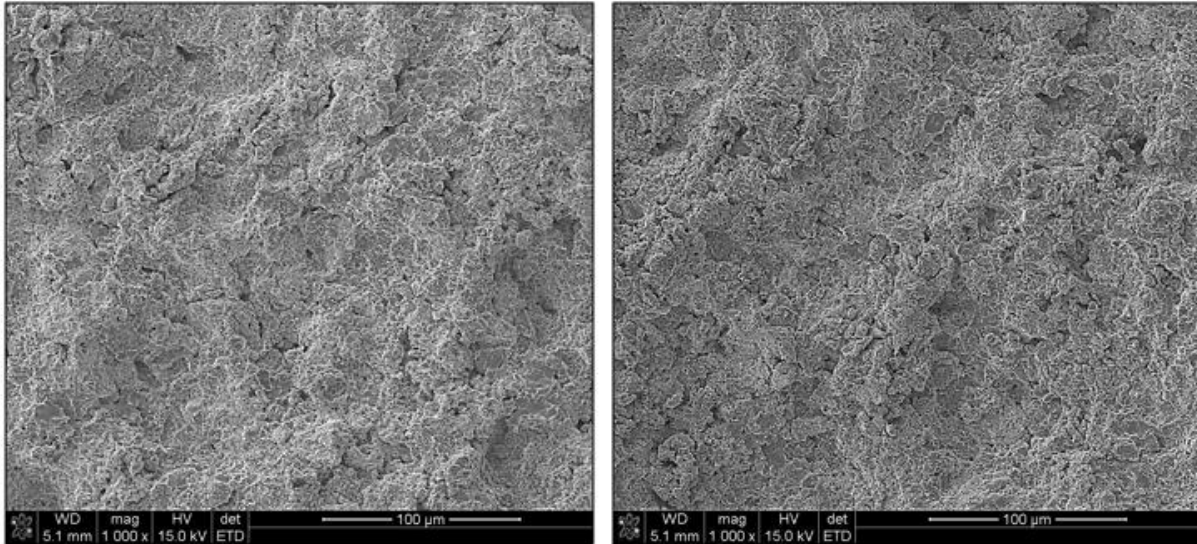
(a)

(b)
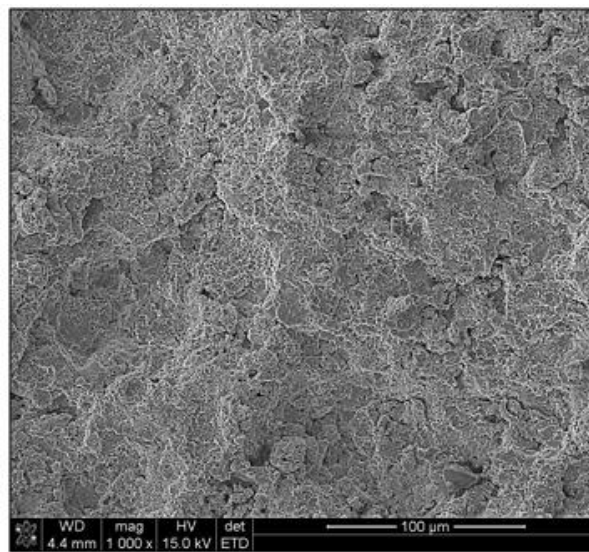
(c)

Fig. 5.1 SEM image of surface after coating (a: 20Ni, b: 25Ni and c: 30Ni)
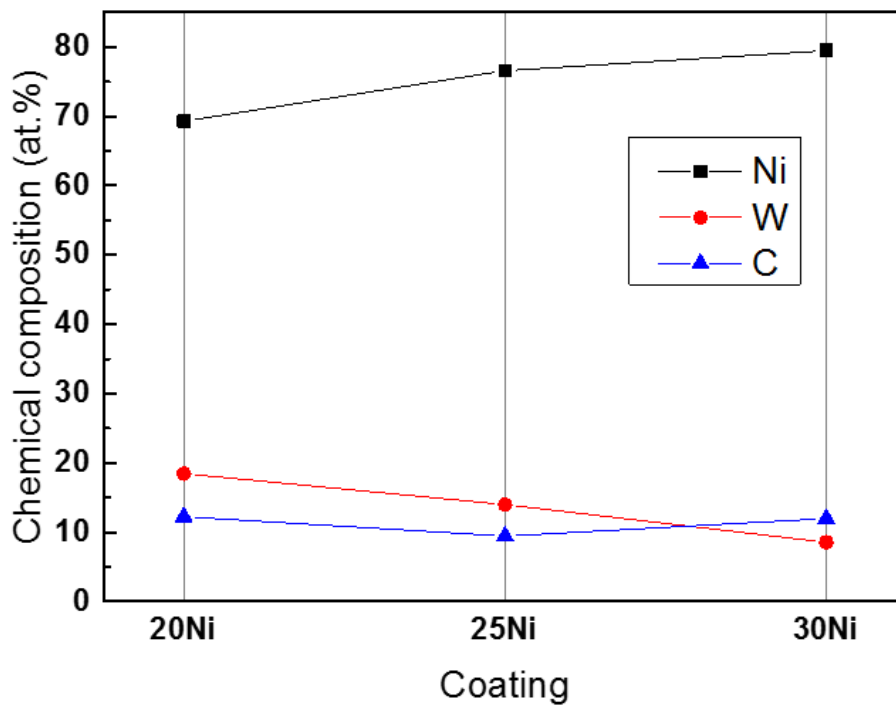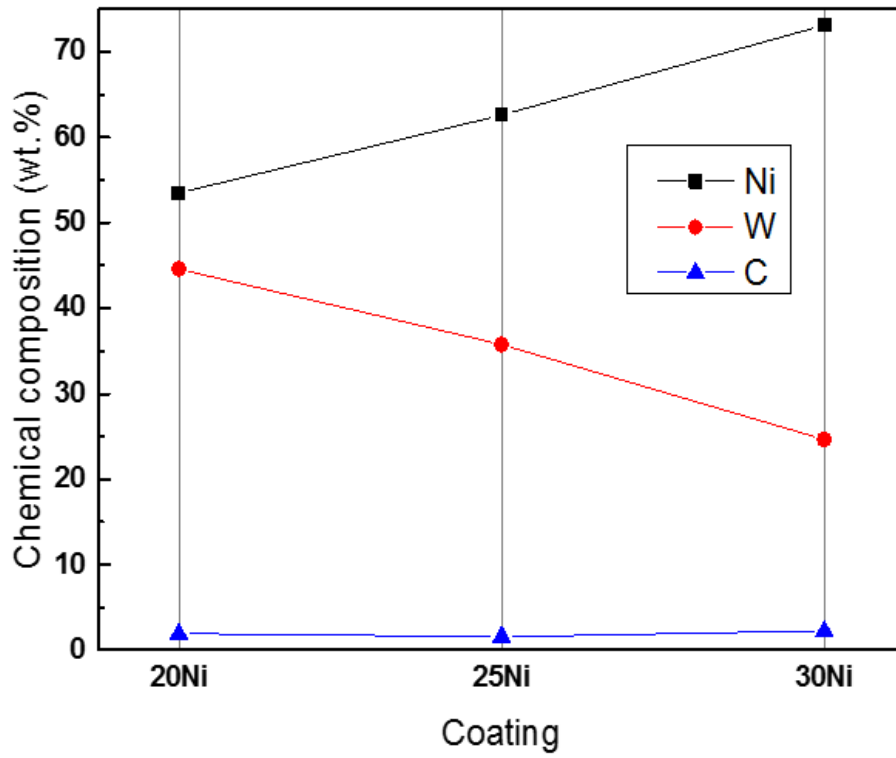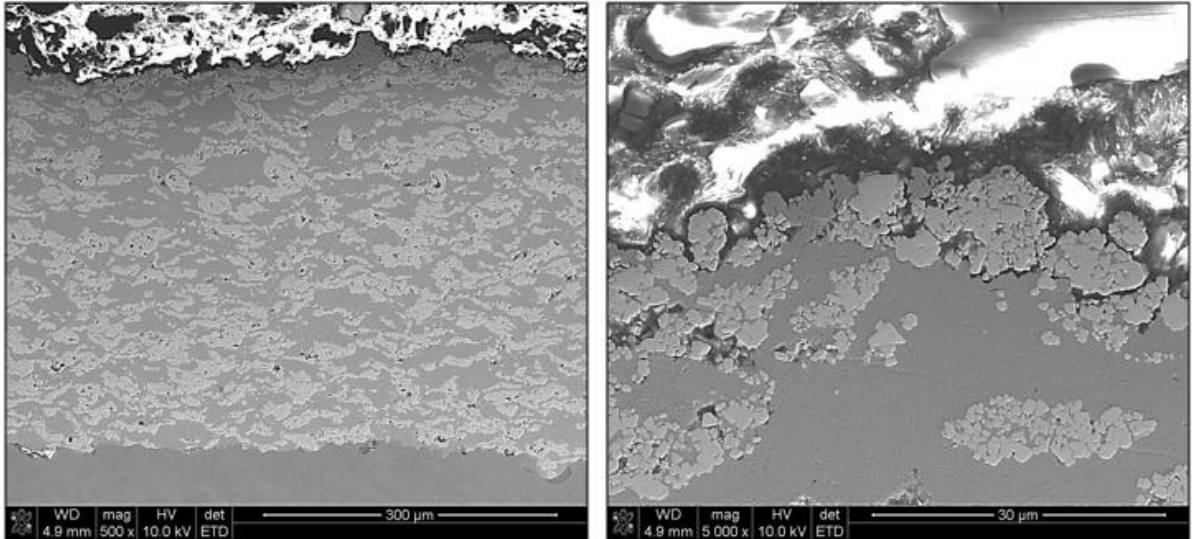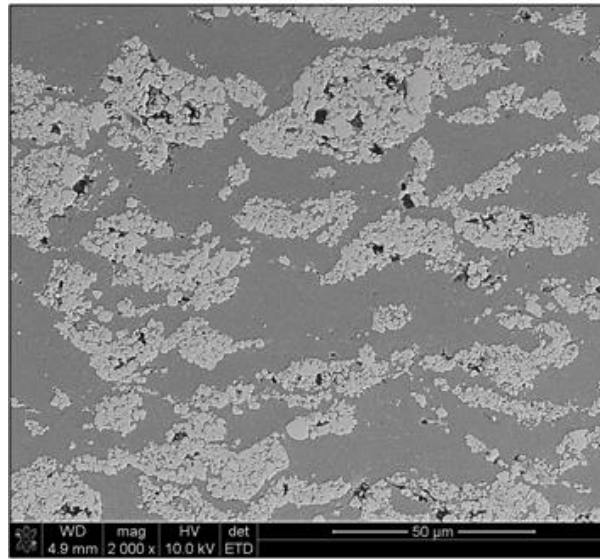
Fig. 5.2 Chemical composition of surface after coating

(a)   (b)

(c)

Fig. 5.3 SEM image of cross-section after 20Ni coating (a: the entire coating layer, b: the surface and c: the central part)
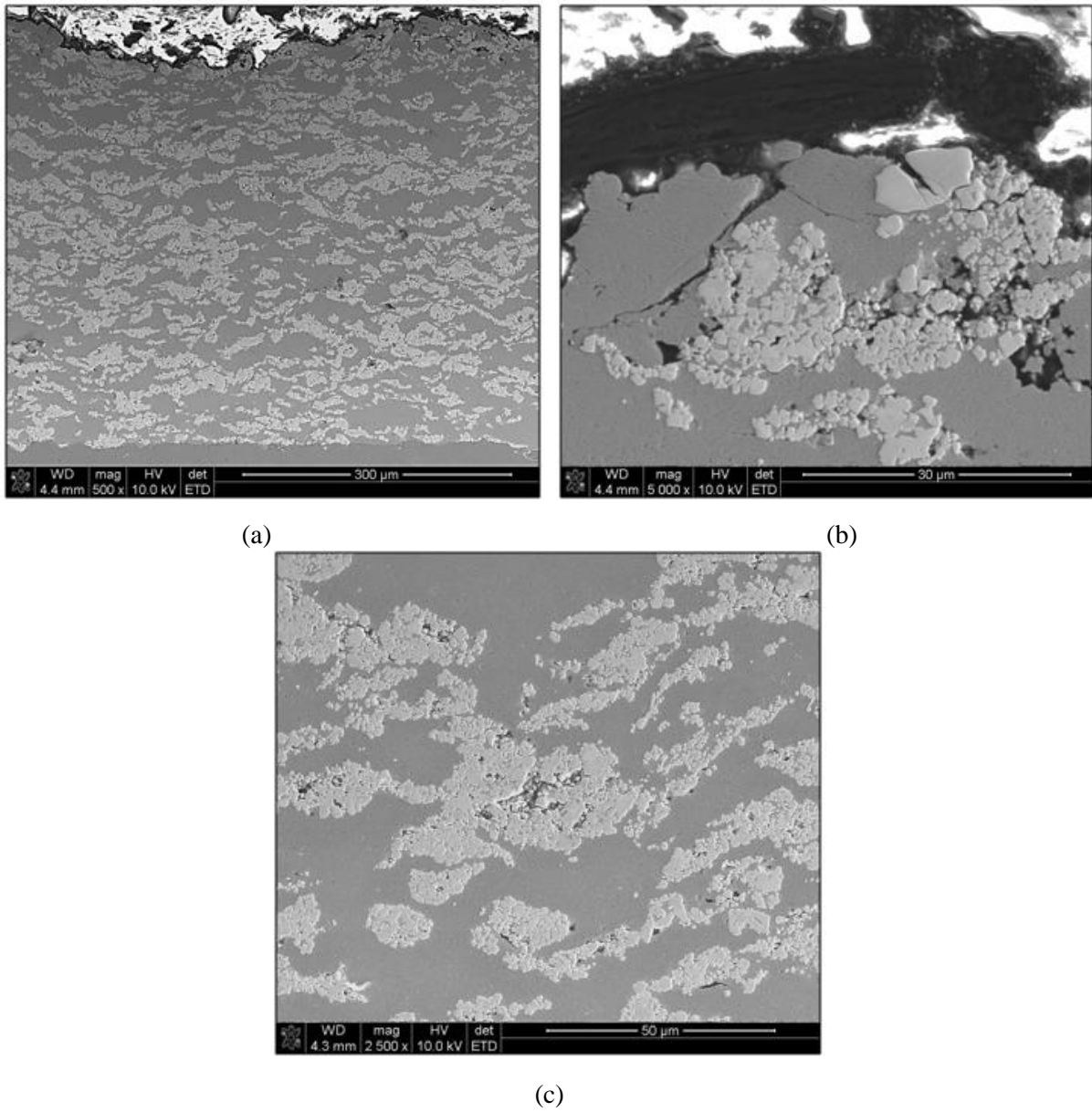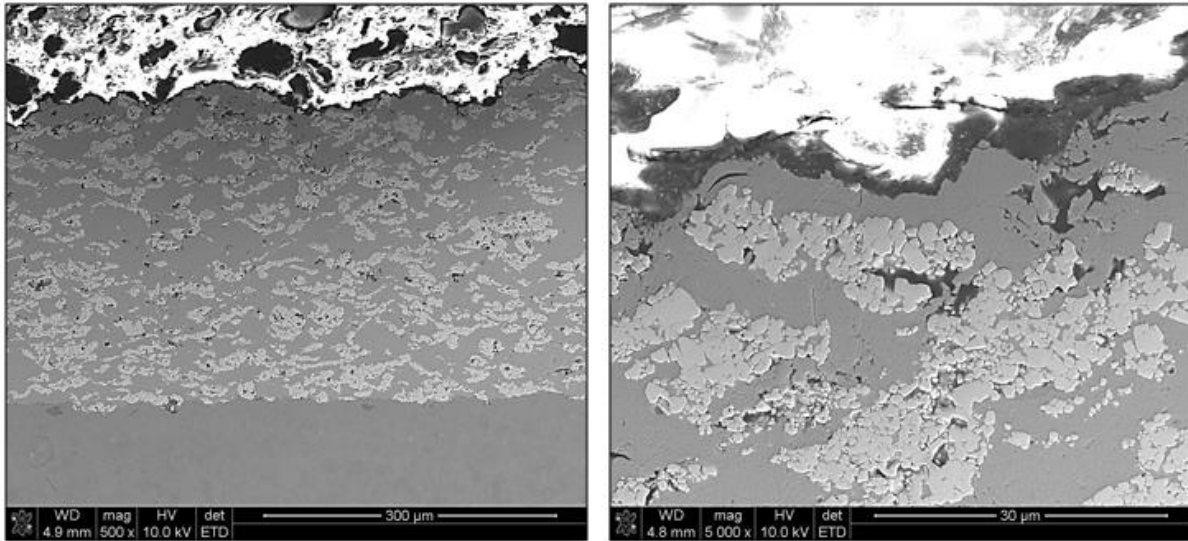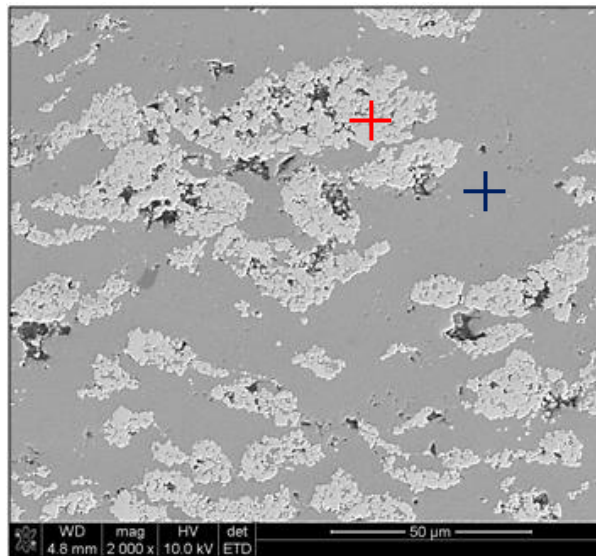
(a)

(b)

(c)

Fig. 5.4 SEM image of cross-section after 25Ni coating (a: the entire coating layer, b: the surface and c: the central part)

(a)

(b)

(c)

Fig. 5.5 SEM image of cross-section after 30Ni coating (a: the entire coating layer, b: the surface and c: the central part)

Table. 5.1 Chemical composition of cross-section at Fig. 5.5

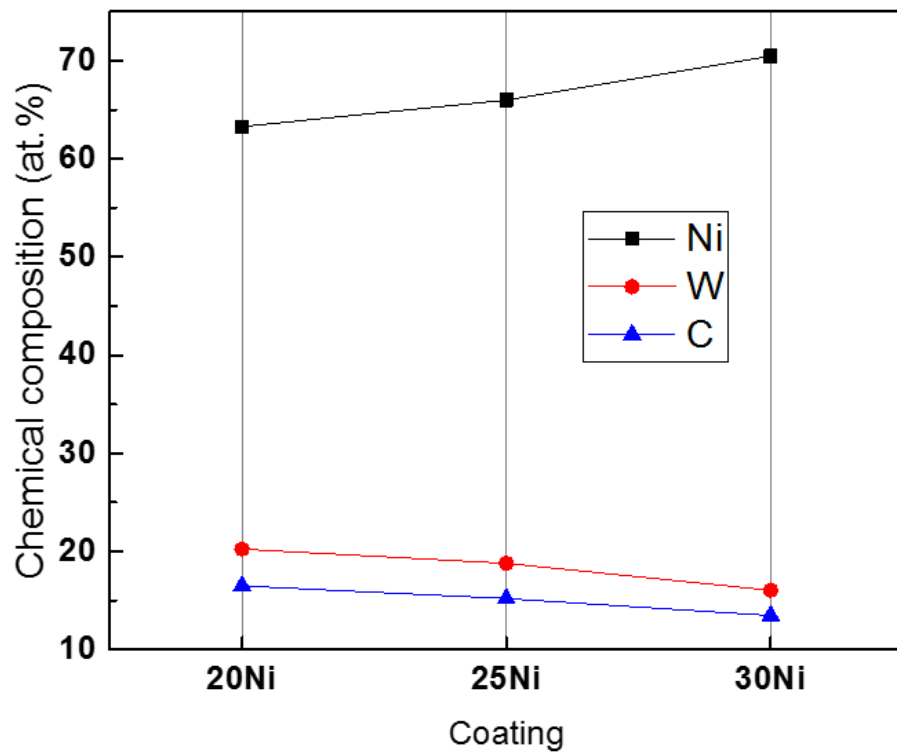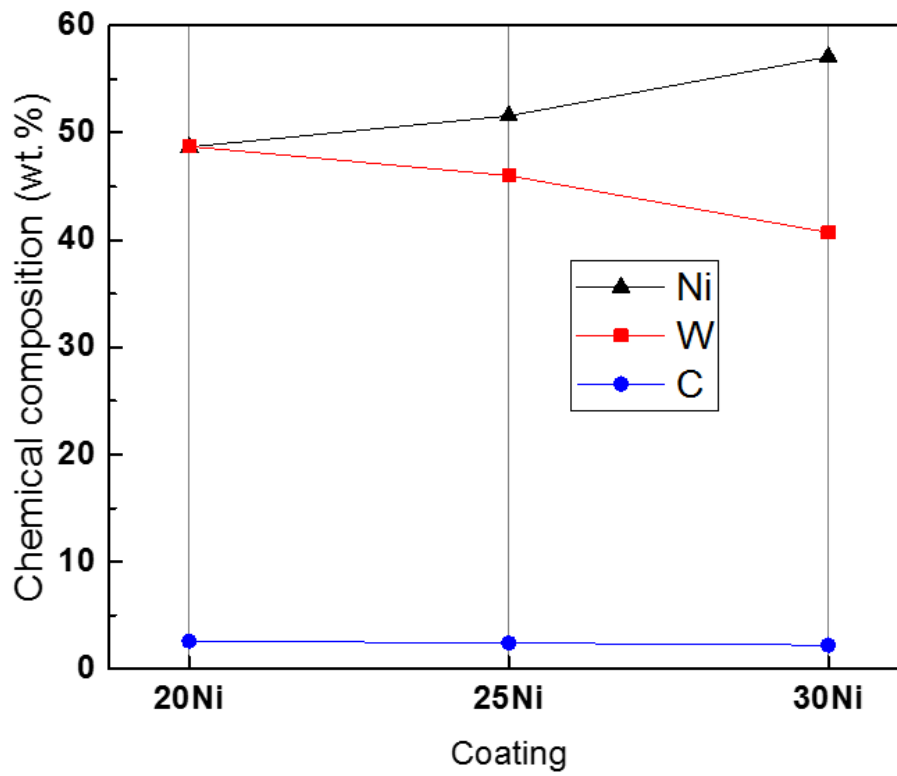| Element	Red		Black	
	wt.%	at.%	wt.%	at.%
Ni	0	0	100	100
W	97	67	0	0
C	3	33	0	0

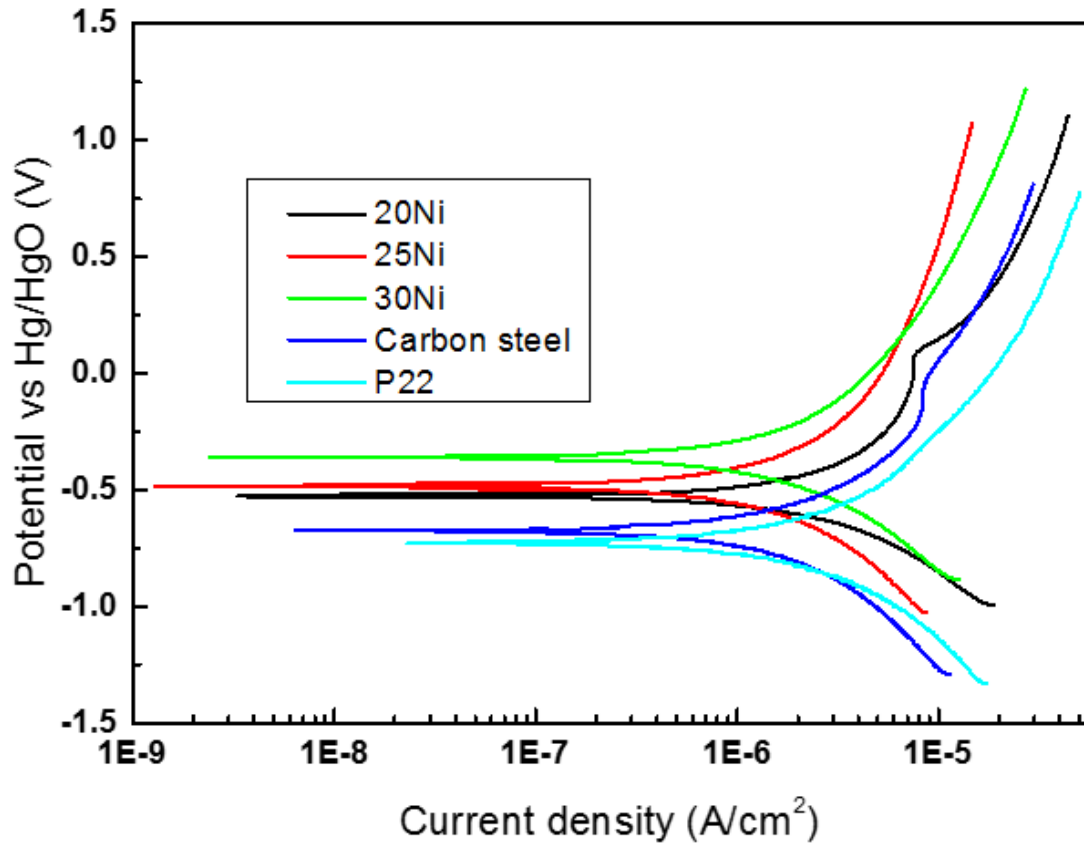Fig. 5.6 Chemical composition of cross-section after coating

Fig. 5.7 Potentiodynamic polarization curves of the samples in pH 9.3 ETA solution at room temperature
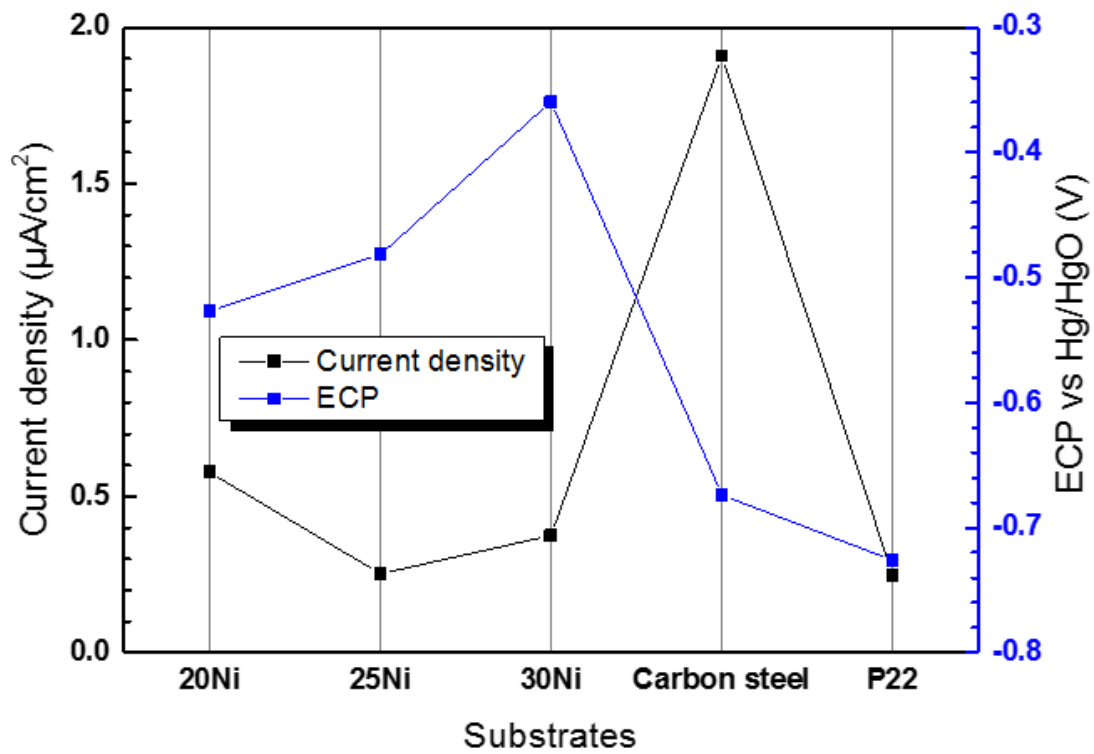
Fig. 5.8 Current density and ECP of substrates in pH 9.3 ETA solution at room temperature

Table. 5.2 Current density and ECP of substrates in pH 9.3 ETA solution at room temperature

	20Ni	25Ni	30Ni	Carbon steel	P22
Current density ($\mu m/cm^2$)	0.58	0.25	0.38	1.91	0.25
ECP vs Hg/HgO (V)	-0.53	-0.48	-0.36	-0.67	-0.73
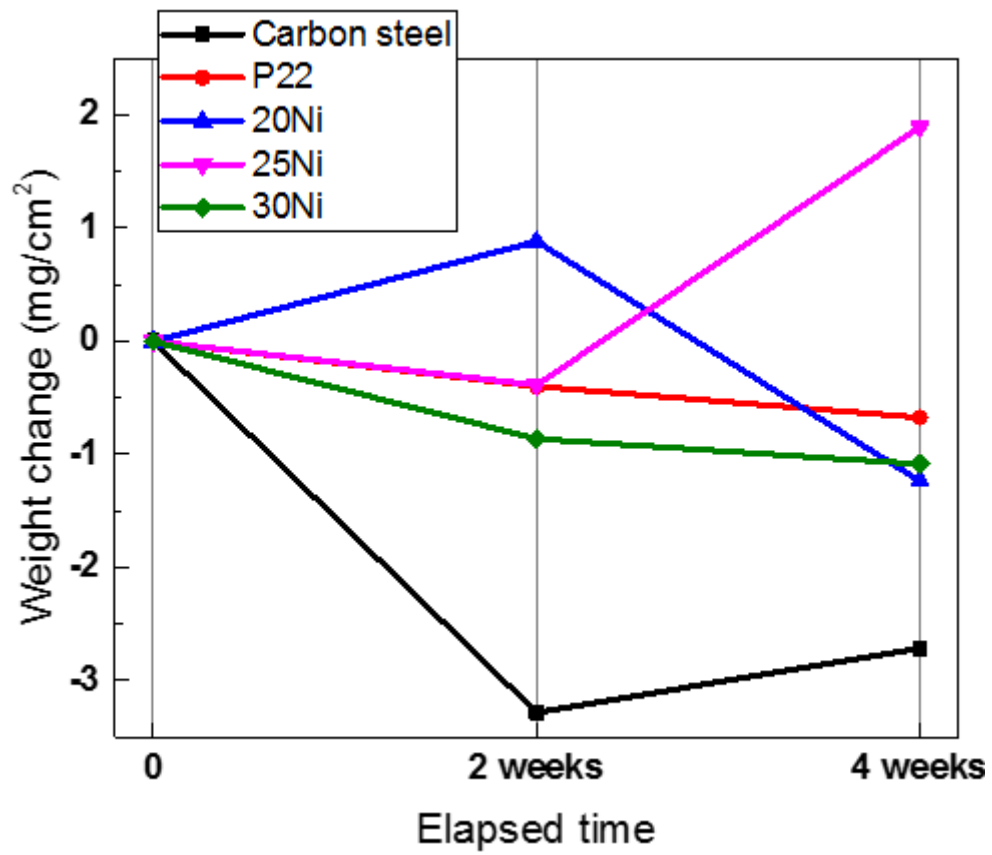
Fig. 5.9 Weight change of coating, carbon steel and P22
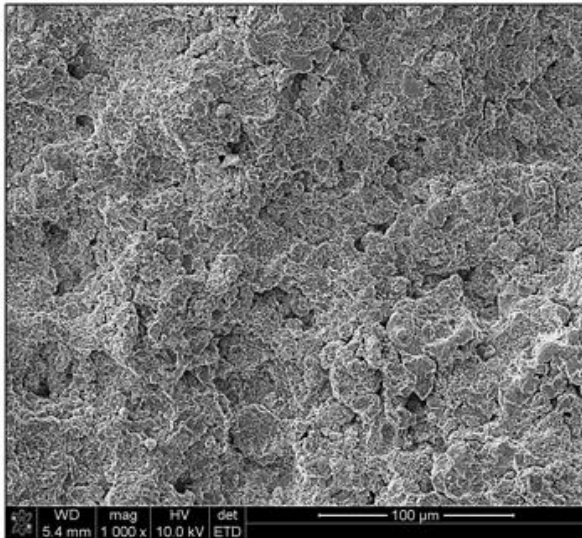
(a)
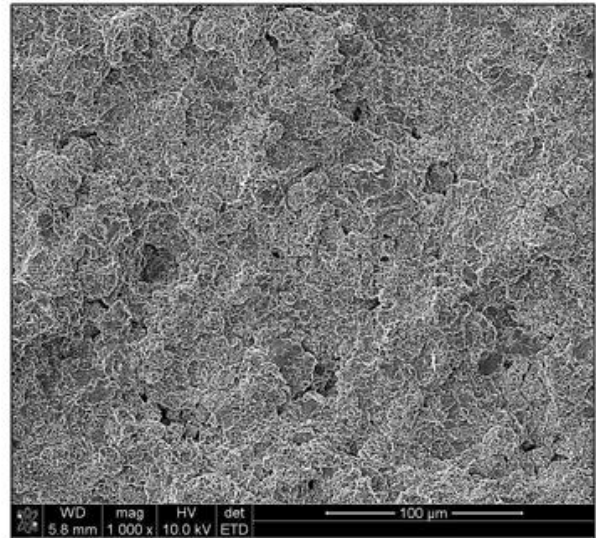
(b)
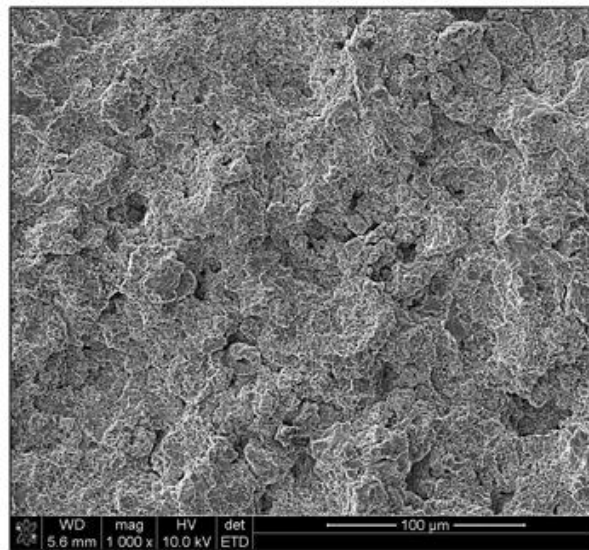
(c)

Fig. 5.10 SEM image of surface after 2 weeks FAC simulation experiments (a: 20Ni coating, b: 25Ni coating and c: 30Ni coating)
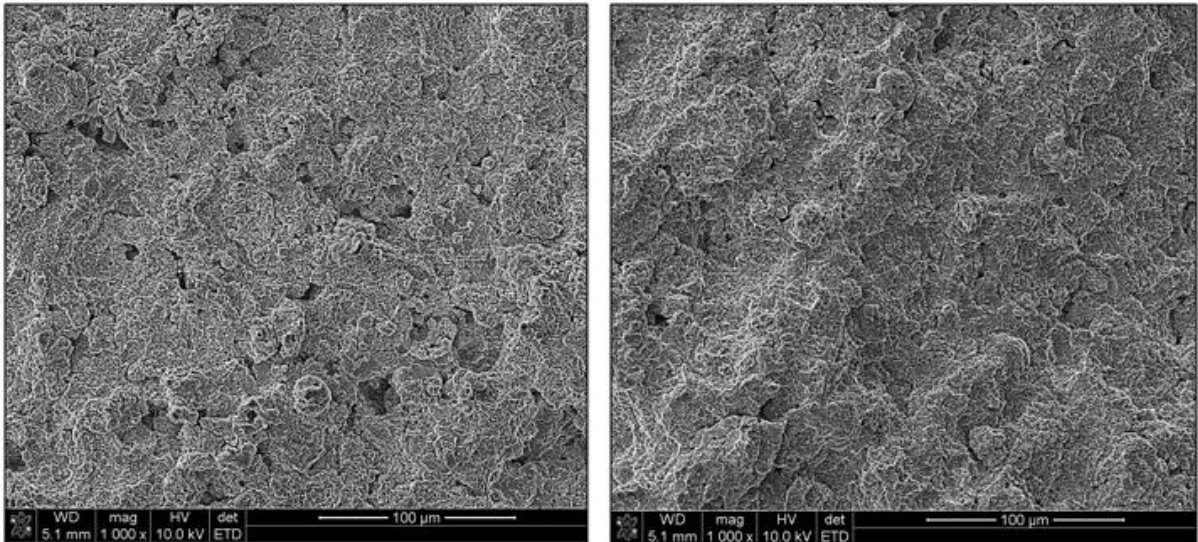
(a)

(b)
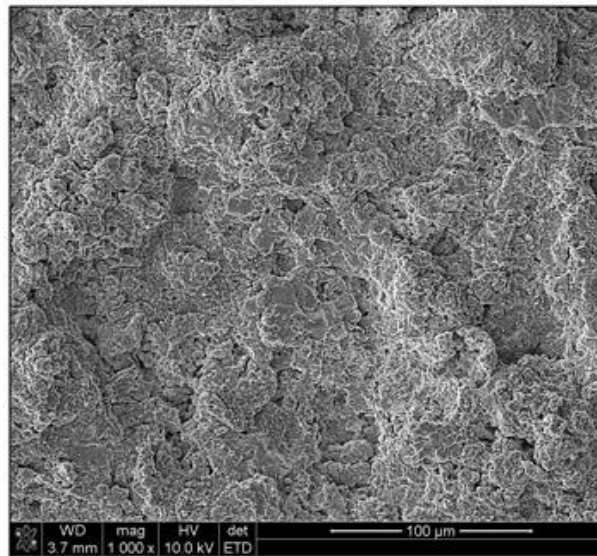
(c)

Fig. 5.11 SEM image of surface after 4 weeks FAC simulation experiments (a: 20Ni coating, b: 25Ni coating and c: 30Ni coating)
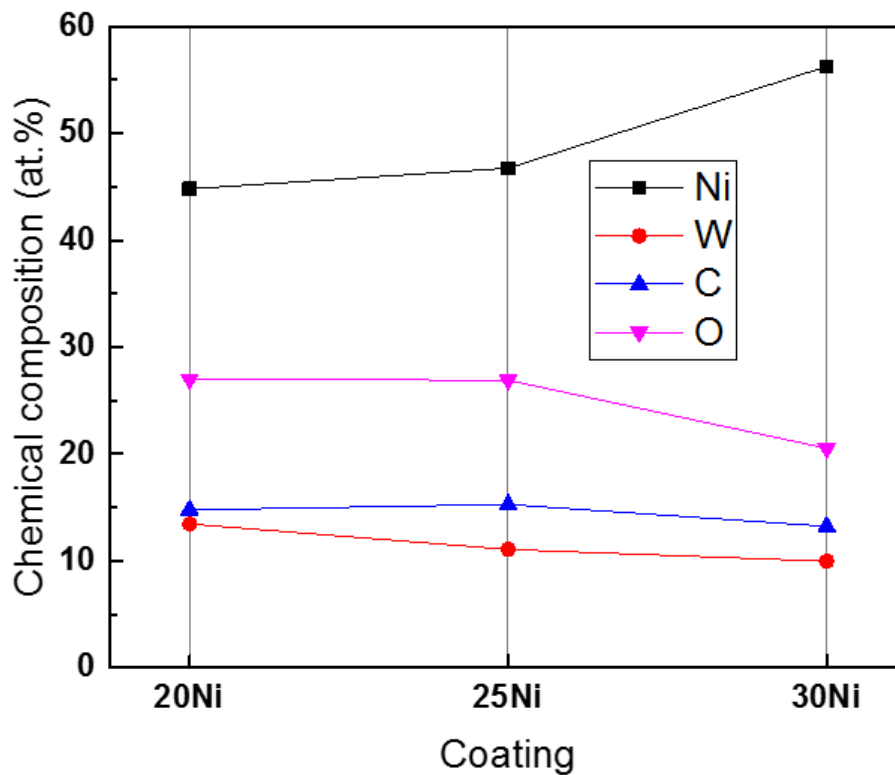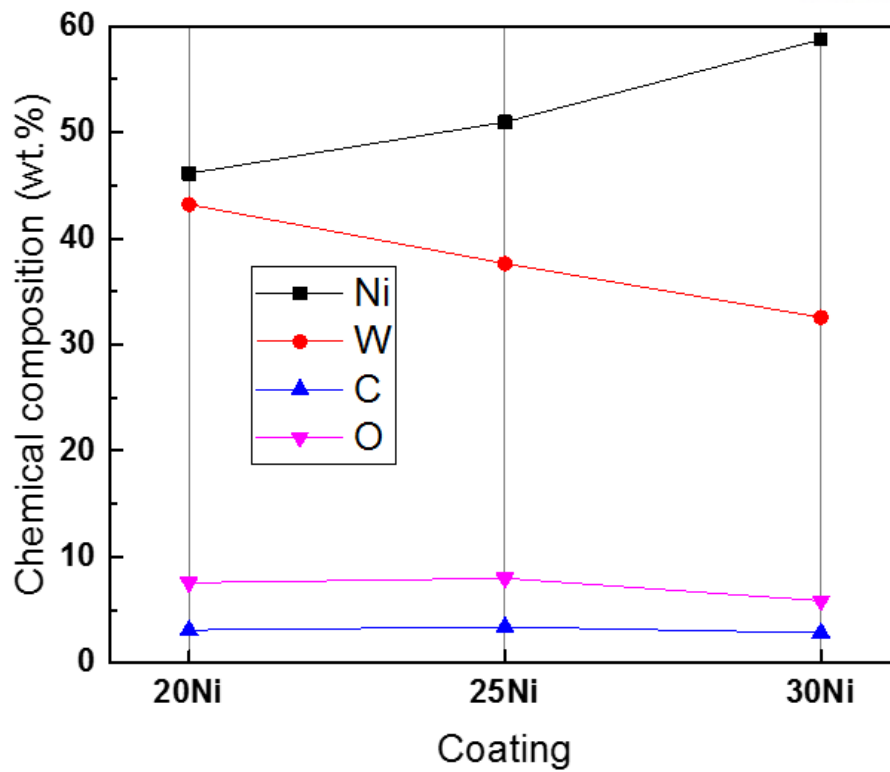
Fig. 5.12 Chemical composition of surface after 2 weeks FAC simulation experiments
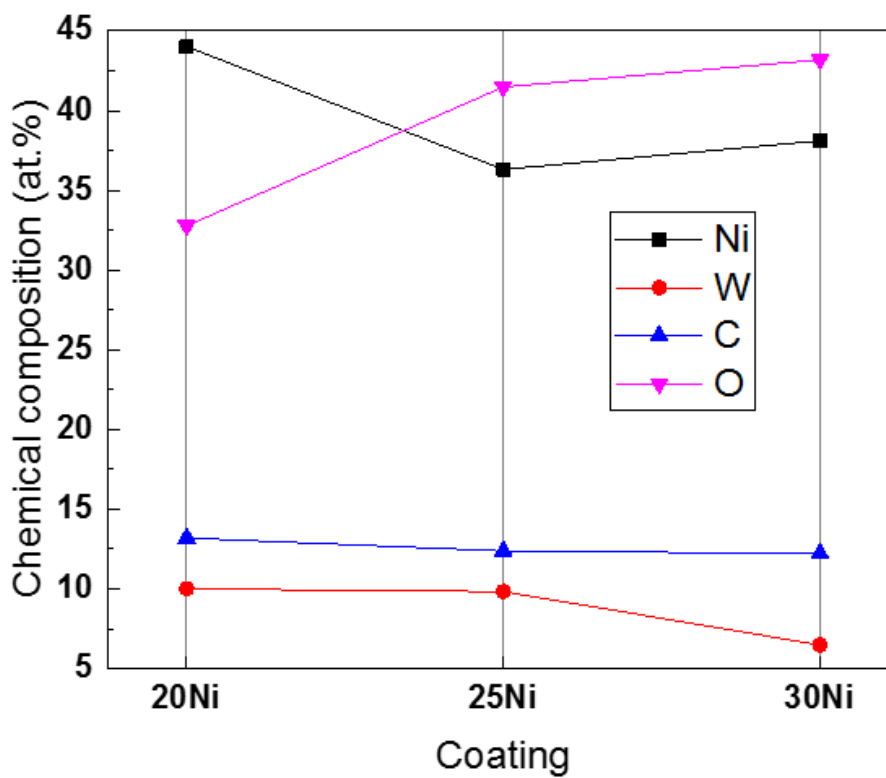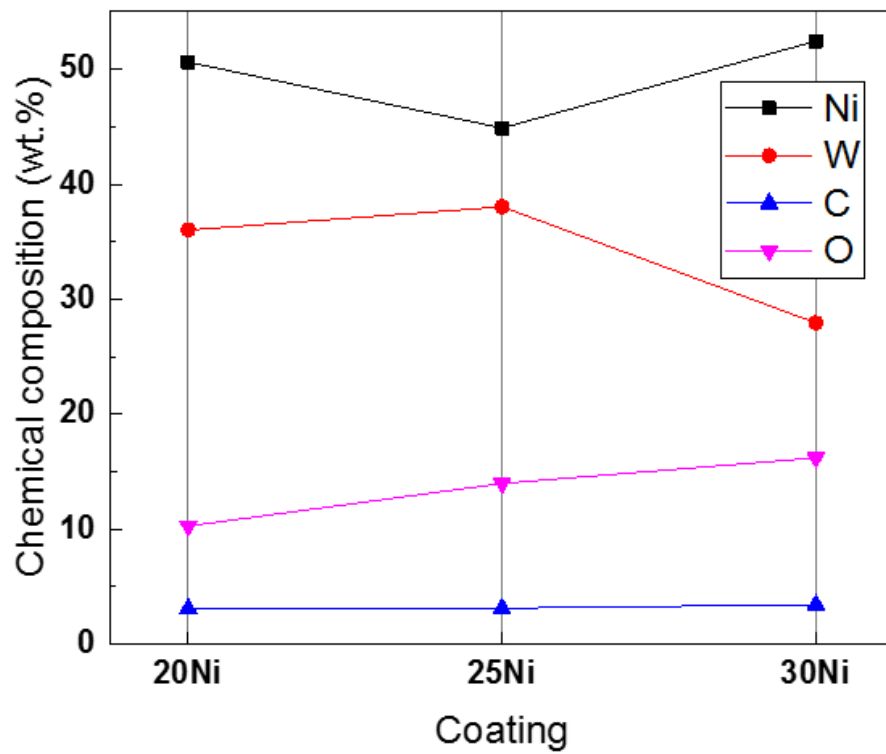
Fig. 5.13 Chemical composition of surface after 4 weeks FAC simulation experiments
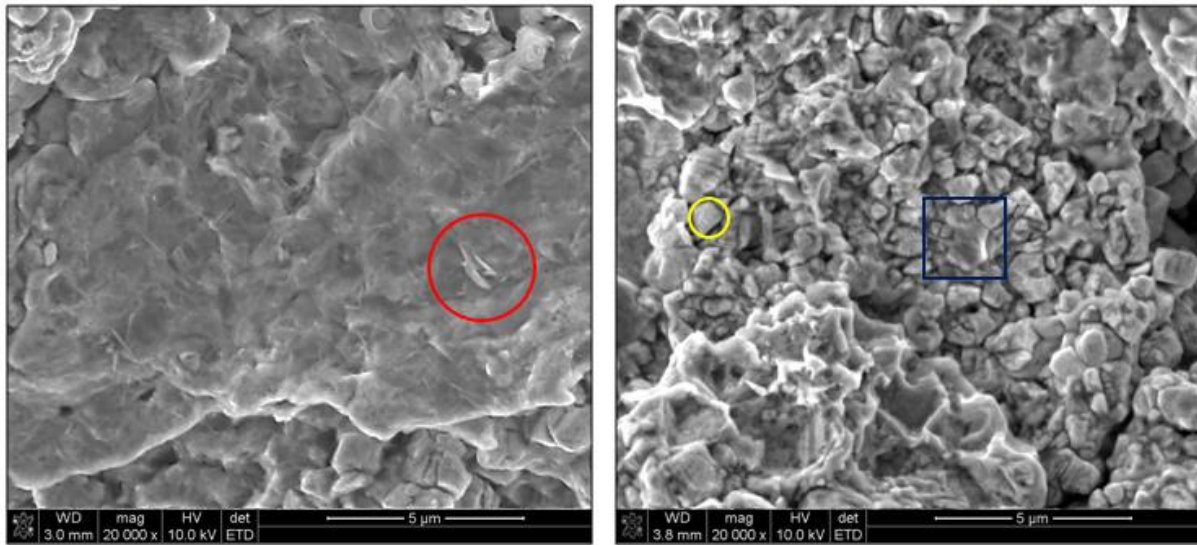
<center>(a)   (b)</center>

Fig. 5.14 SEM image of surface after FAC simulation experiments (a: 20Ni coating after 2 weeks and b: 20Ni coating after 4 weeks)

Table. 5.3 Chemical composition of red circle at Fig. 5.14

Element	wt.%	at.%
Ni	69.08	44.10
W	07.73	01.58
O	23.19	54.32

Table. 5.4 Chemical composition of yellow circle at Fig. 5.14

Element	wt.%	at.%
Ni	05.74	09.62
W	88.34	47.24
O	02.61	16.03
C	03.31	27.11

Table. 5.5 Chemical composition of blue rectangular at Fig. 5.14

| Element	wt.%	at.%
Ni	23.75	29.03
W	67.10	26.19
O	06.66	29.86
C	02.50	14.92
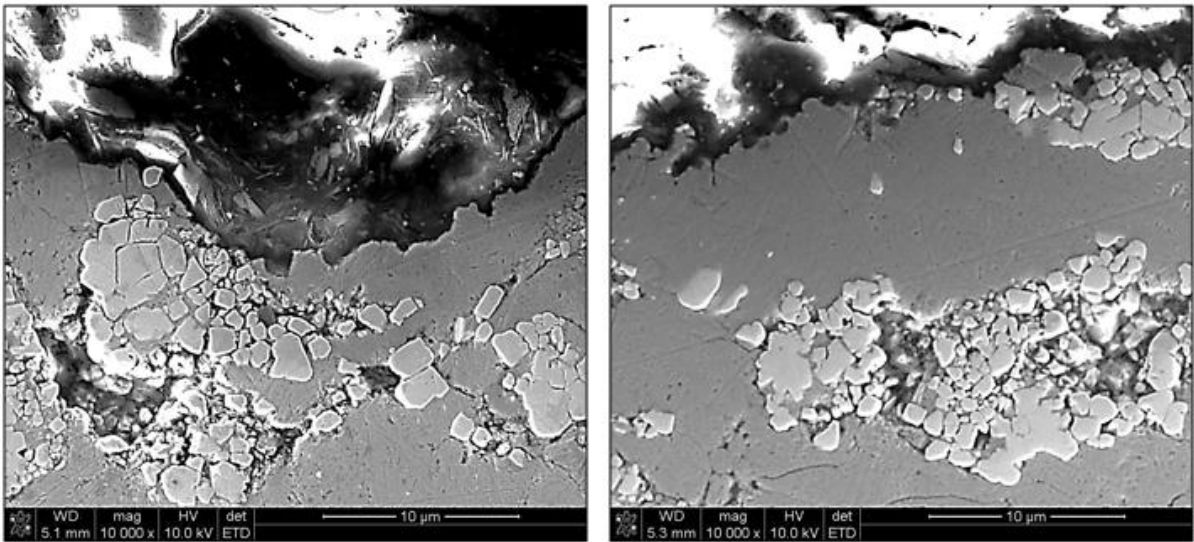
(a)

(b)
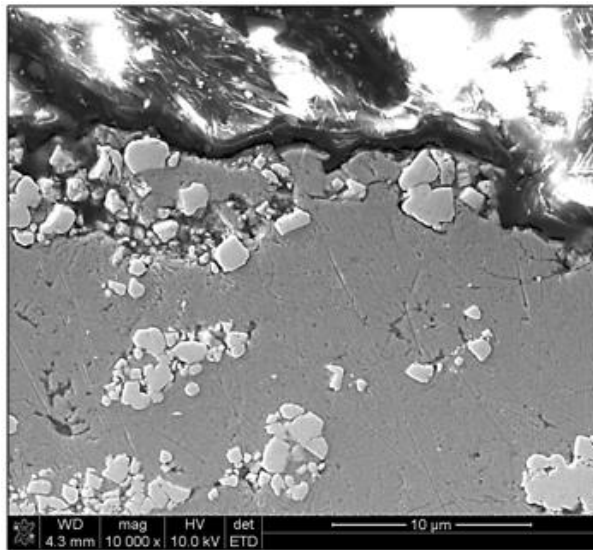
(c)

Fig. 5.15 SEM image of cross-section after 2 weeks FAC simulation experiments (a: 20Ni coating, b: 25Ni coating and c: 30Ni coating)
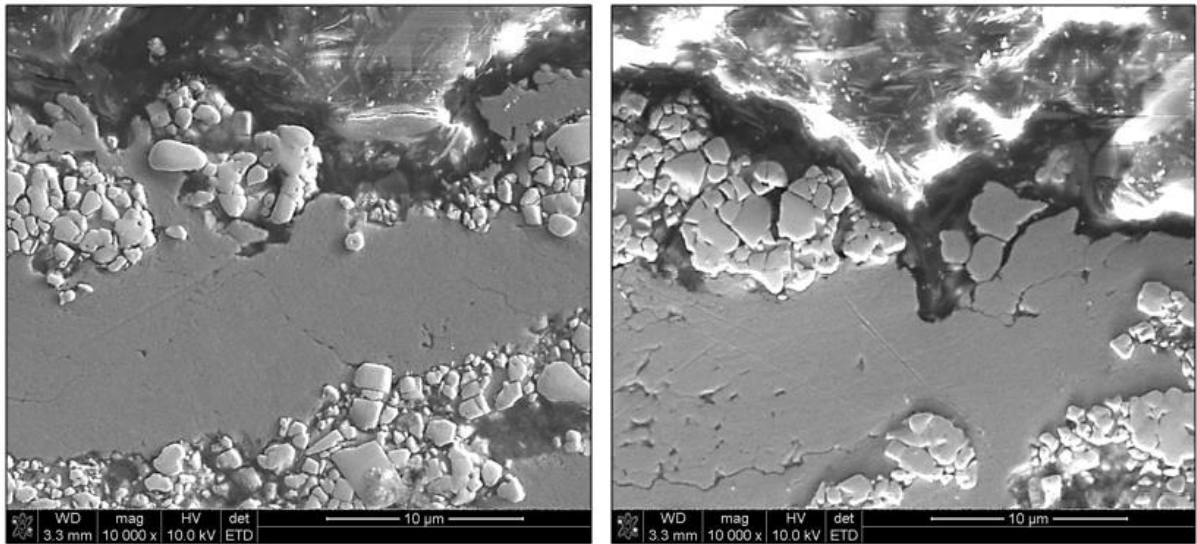
(a)

(b)
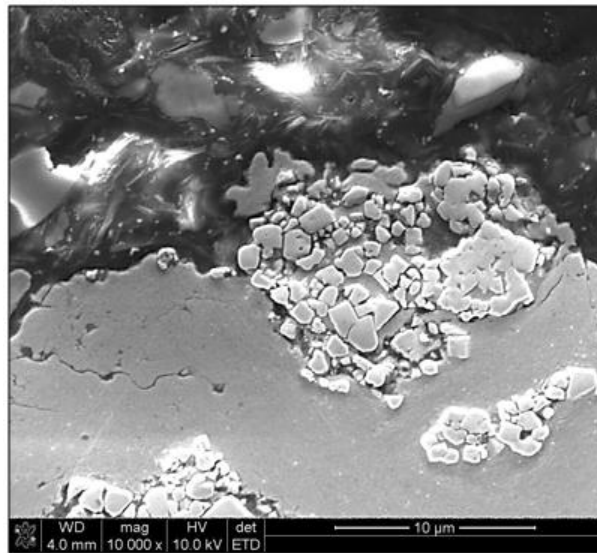
(c)

Fig. 5.16 SEM image of cross-section after 4 weeks FAC simulation experiments (a: 20Ni coating, b: 25Ni coating and c: 30Ni coating)
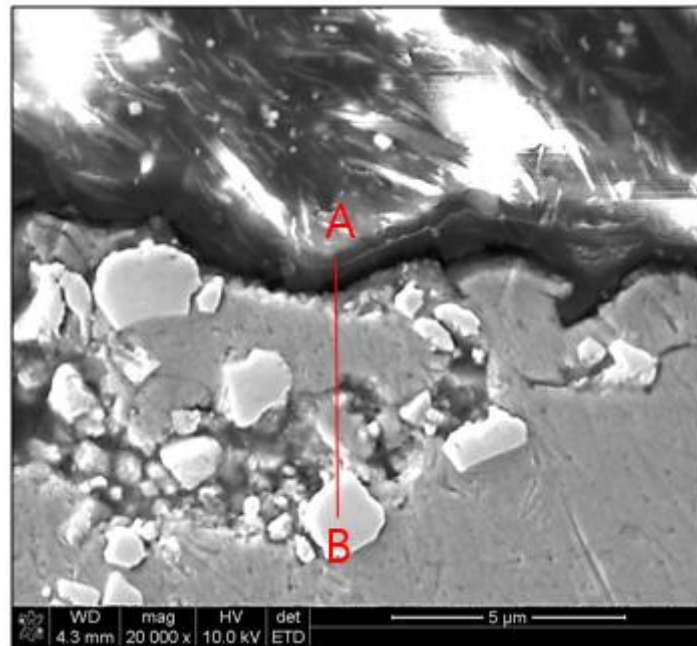
Fig. 5.17 SEM image of cross-section after 2 weeks FAC simulation experiments (30Ni coating)
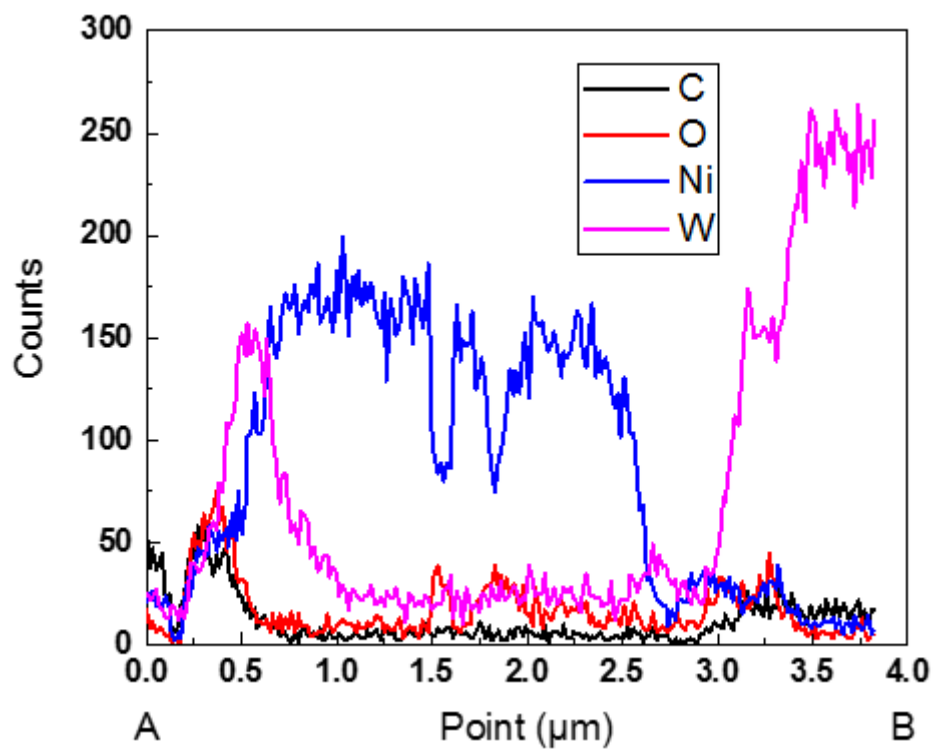
Fig. 5.18 Line EDS analysis of cross-section of 30Ni coating after 2 weeks FAC simulation
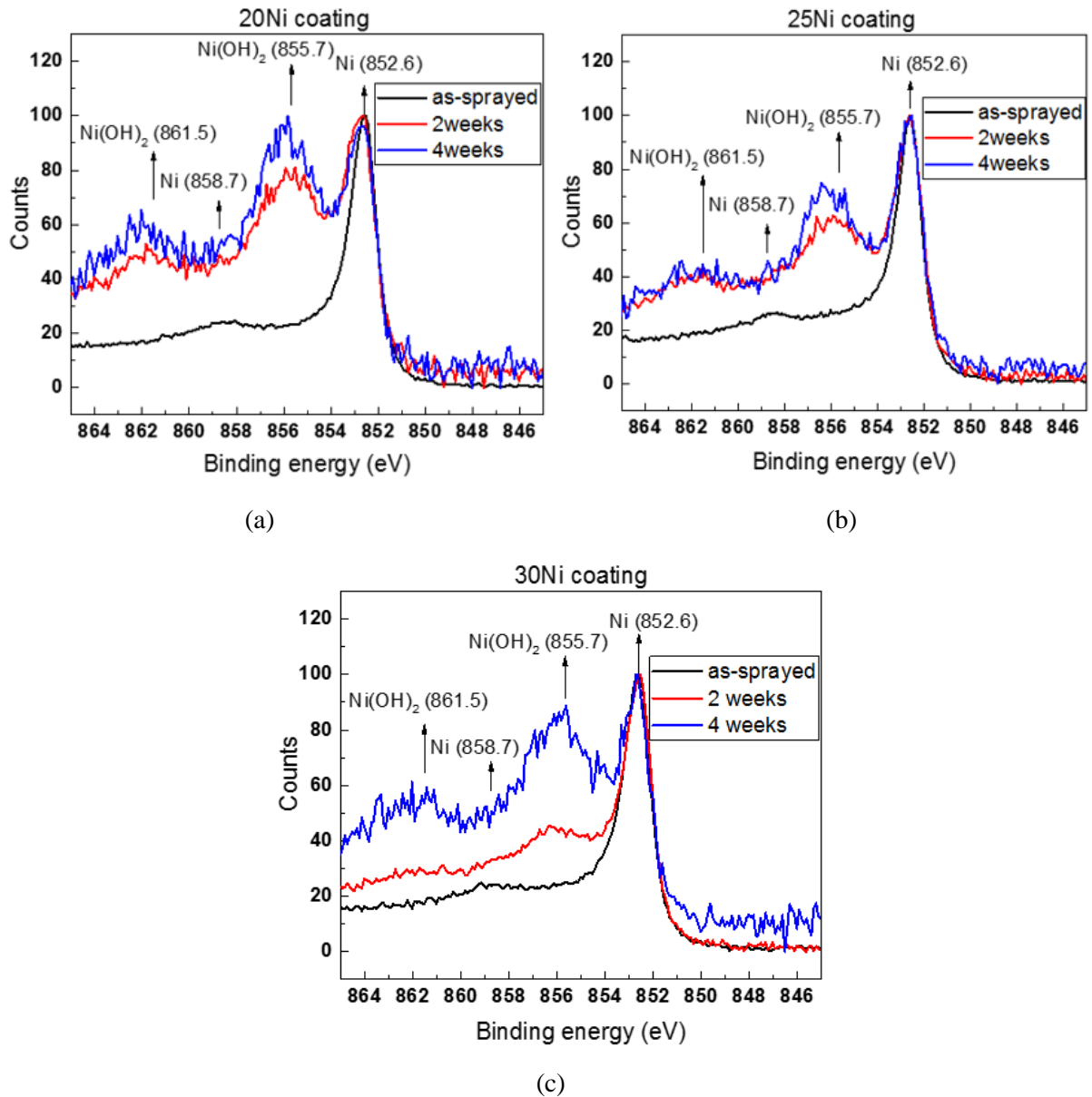
Fig. 5.19 XPS data of Ni after 420 s etching (a: 20Ni, b: 25Ni c: 30Ni coating)
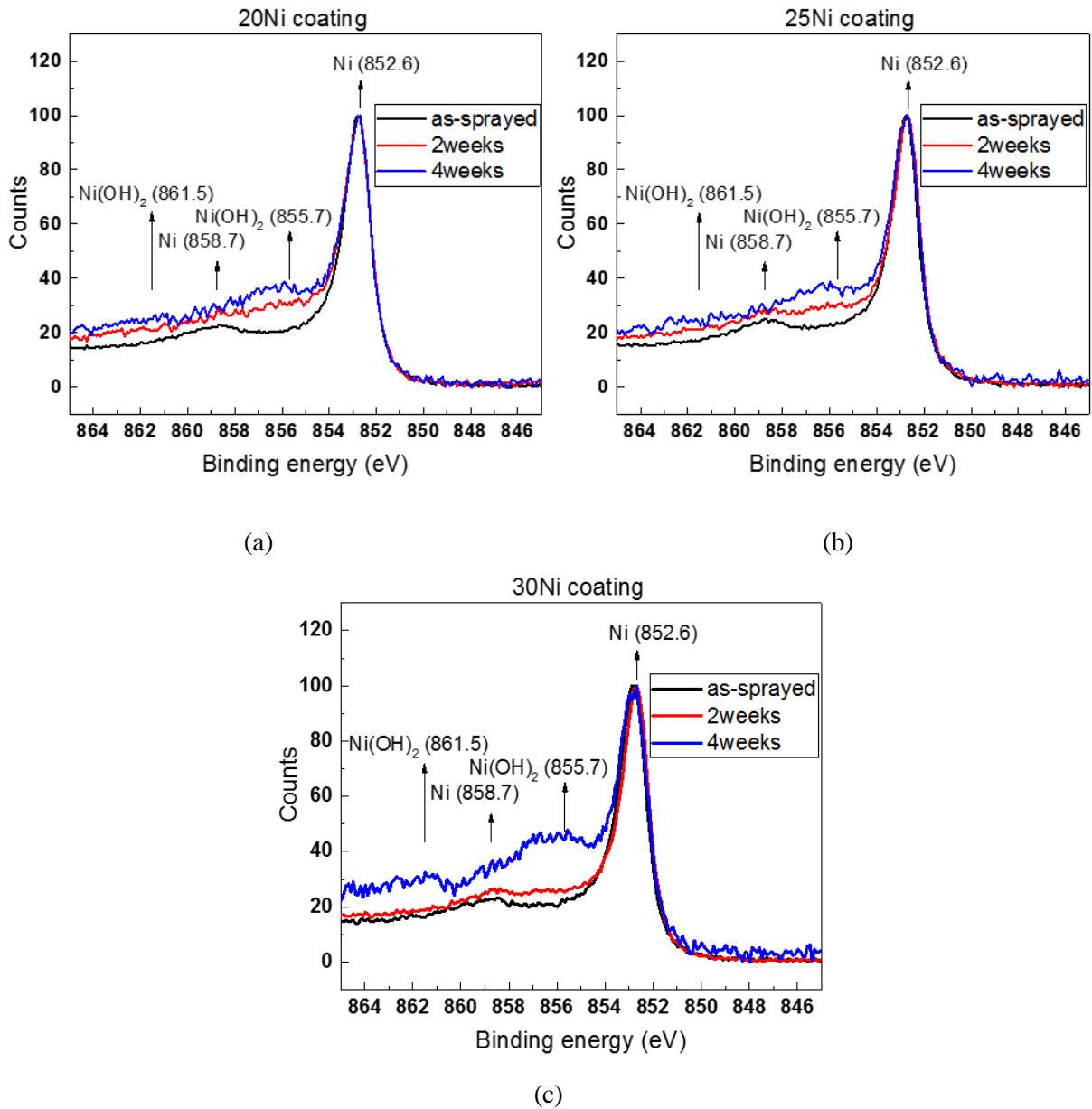
Fig. 5.20 XPS data of Ni after 2020 s etching (a: 20Ni, b: 25Ni c: 30Ni coating)
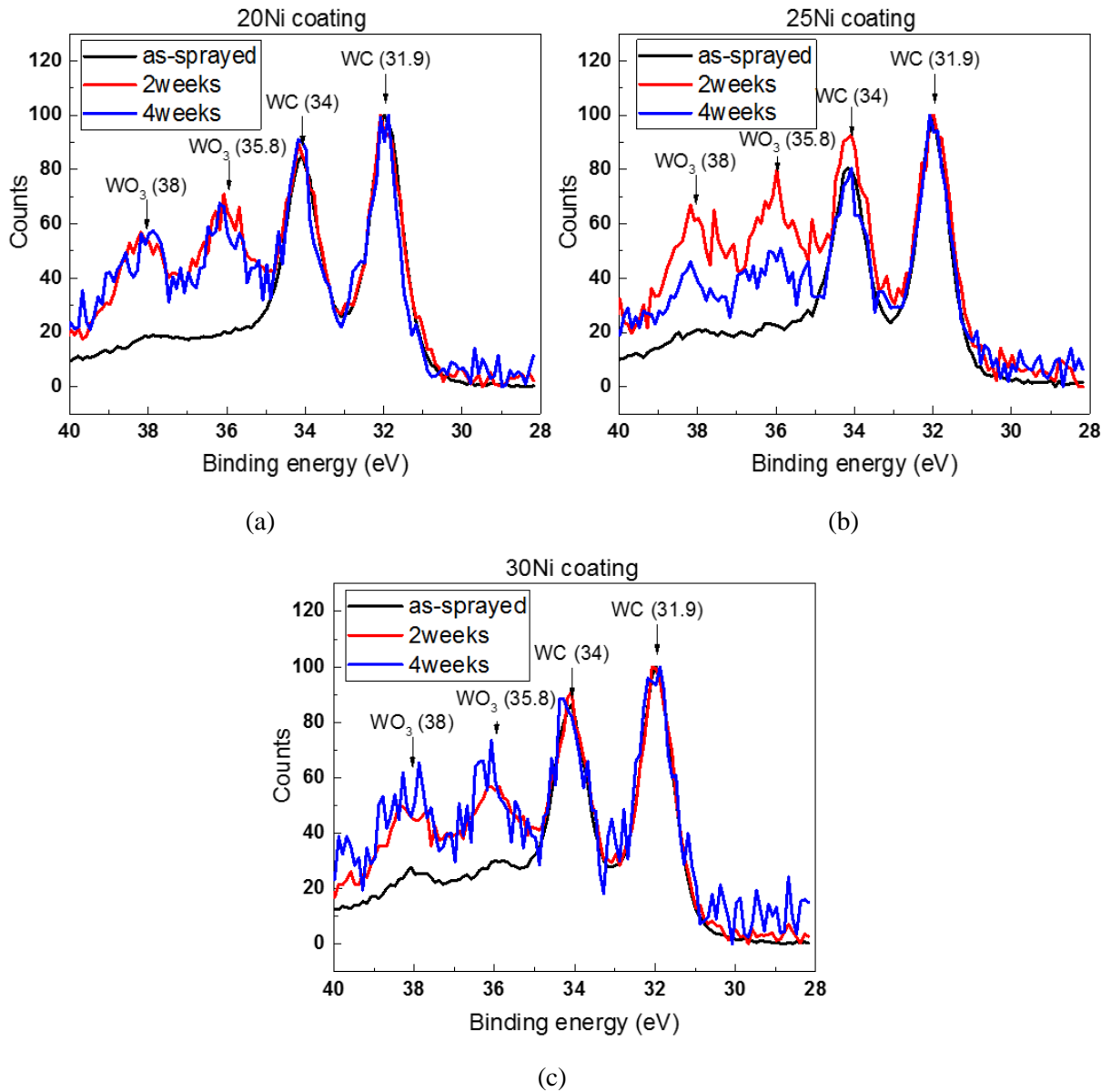
Fig. 5.21 XPS data of W after 420 s etching (a: 20Ni, b: 25Ni c: 30Ni coating)
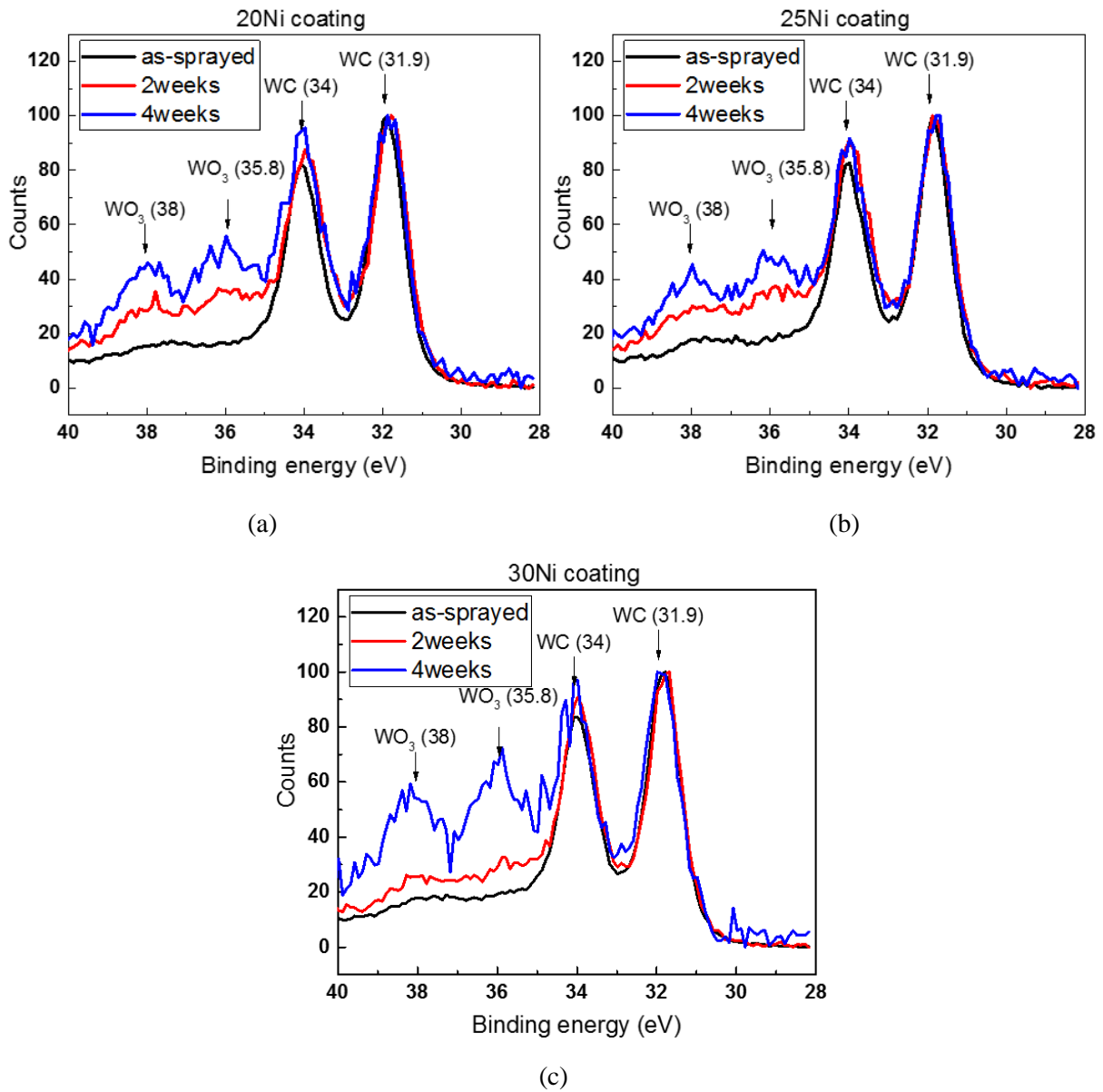
Fig. 5.22 XPS data of W after 2020 s etching (a: 20Ni, b: 25Ni c: 30Ni coating)

VI. Discussion

6.1 Chemical composition

Powders used at coating are Ni and WC-10Ni particle. Therefore, characteristic at surface of coating is changed after FAC simulation experiments. EDS data from precipitation at Ni matrix which is summarized at Table 5.3 indicates oxidation products of Ni are generated after FAC simulation test. However, oxidation products of Ni cannot be uniformly formed above Ni matrix. At the regions where WC-10Ni is coated, high Ni region and low Ni region is coexisting. The low Ni region such as yellow circle at Fig. 5.14 indicates Ni acting as binder metal is dissolved and WC exists only at a part of surface. According to Zimniak et al [46], the reason of Ni dissolution is low thermal stability of $Ni(OH)_2$ at high temperature. At high temperature solution, pH decrease and low thermal stability induces dissolution of $Ni(OH)_2$.

$$Ni(OH)_2 \ + \ 2H^+ \ \leftrightarrow Ni^{2+} + 2H_2O \tag{22}$$
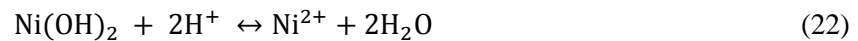
Because of higher reduction potential of WC than Ni [2, 37, 38], it leads galvanic corrosion of Ni acting like a sacrificial metal to WC. Therefore, WC oxidation process is suppressed and $Ni(OH)_2$ is formed at early stages of corrosion process. As a results, dissolution of $Ni(OH)_2$ occurs after corrosion of Ni at high temperature because WC has high corrosion resistance to hydrogen ion [37, 38]. The results of SEM images and discussion is summarized by schematic view of coating surface at Fig. 6.1

6.2 Weight change

The corrosion process of cemented carbide is results of galvanic corrosion of binder metal [47]. From WC-Co dissolution experiments [48], pH increases at early stage of corrosion and suddenly decreases at neutral water. This phenomenon indicates binder metal dissolution of cemented carbide is dominant reaction first and suppresses WC dissolution. In high temperature oxidation experiments [49], selective oxidation of binder metal occurs first at the early stage of oxidation.

For detecting dissolution of binder metal at FAC experiments, the proportion of Ni and W is calculated from SEM EDS data and presented in Fig. 6.2. The ratio of Ni to Ni and W is decreased after 2 weeks.

Decreases indicates galvanic corrosion of Ni is dominant reaction and Ni is dissolved to water. Therefore, increases of Ni contents in coating effect on corrosion and weight change of coating in early stage oxidation. Increases of Ni contents mean dissolution of Ni occurs more than before. However, because of lower Ni contents at 20Ni coating than other coating, galvanic corrosion of Ni at 20Ni coating occur less than that at other coating. As a results, oxidation of WC induces weight gain.

After 4 weeks FAC simulation, weight change of coating is similar with W chemical composition. In case of 20Ni coating, low Ni contents in coating accelerates WC oxidation before 2 weeks so oxidation products, WO3, is dissolved to water at 4 weeks. Therefore, proportion of W is decreased. However, higher Ni contents at other coating than 20Ni coating delay the oxidation of WC and these effect is observed at 4 weeks. Consequently, the ratio of W at 25Ni and 30Ni coating is slightly decreased or increased after 4 weeks

6.3 Oxidation of nickel and tungsten carbide

The proportion of oxidation products of Ni and W at Fig. 6.3 reveals that the tendency of corrosion at 20Ni coating surface is different from 25Ni and 30Ni coating surface. WO_3 dissolution at 20Ni coating caused by the absence of Ni matrix occurs at 4 weeks and the proportion of WC compared with WO_3 is increased. Therefore, it induces weight loss of 20Ni coating at 4 weeks. However, increases of WO_3 at 25Ni and 30Ni coating indicates weight change of coating after 4 weeks FAC experiments are result from WC oxidation.

6.4 Corrosion properties

Experimental results after FAC simulation test and mpy calculation by potentiodynamic polarization experiments explain that coating has better corrosion properties than carbon steel.

In addition, comparing to P22 as substitution to carbon steel, mpy of 25Ni coating at Fig. 6.4 is 2.02 μm/yr and 2.27 μm/yr is calculated from 30Ni coating which values are smaller than P22 (2.84 μm/yr). It has same results at FAC simulation experiments.

Therefore, 25Ni coating has better performance about corrosion than carbon steel and P22.

WC and WO$_3$ dissolution

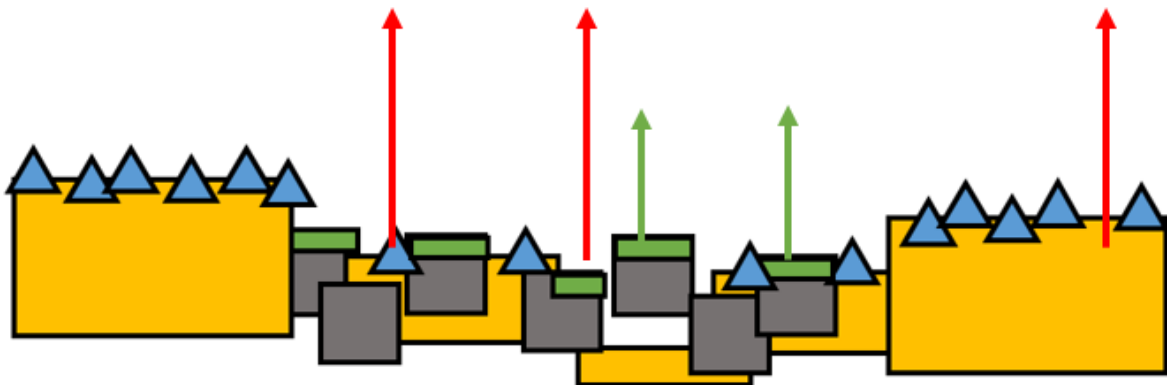Ni(OH)$_2$ dissolution

Ni   WC

Ni(OH)$_2$ WO$_3$

Fig. 6.1 Schematic view of corrosion at surface
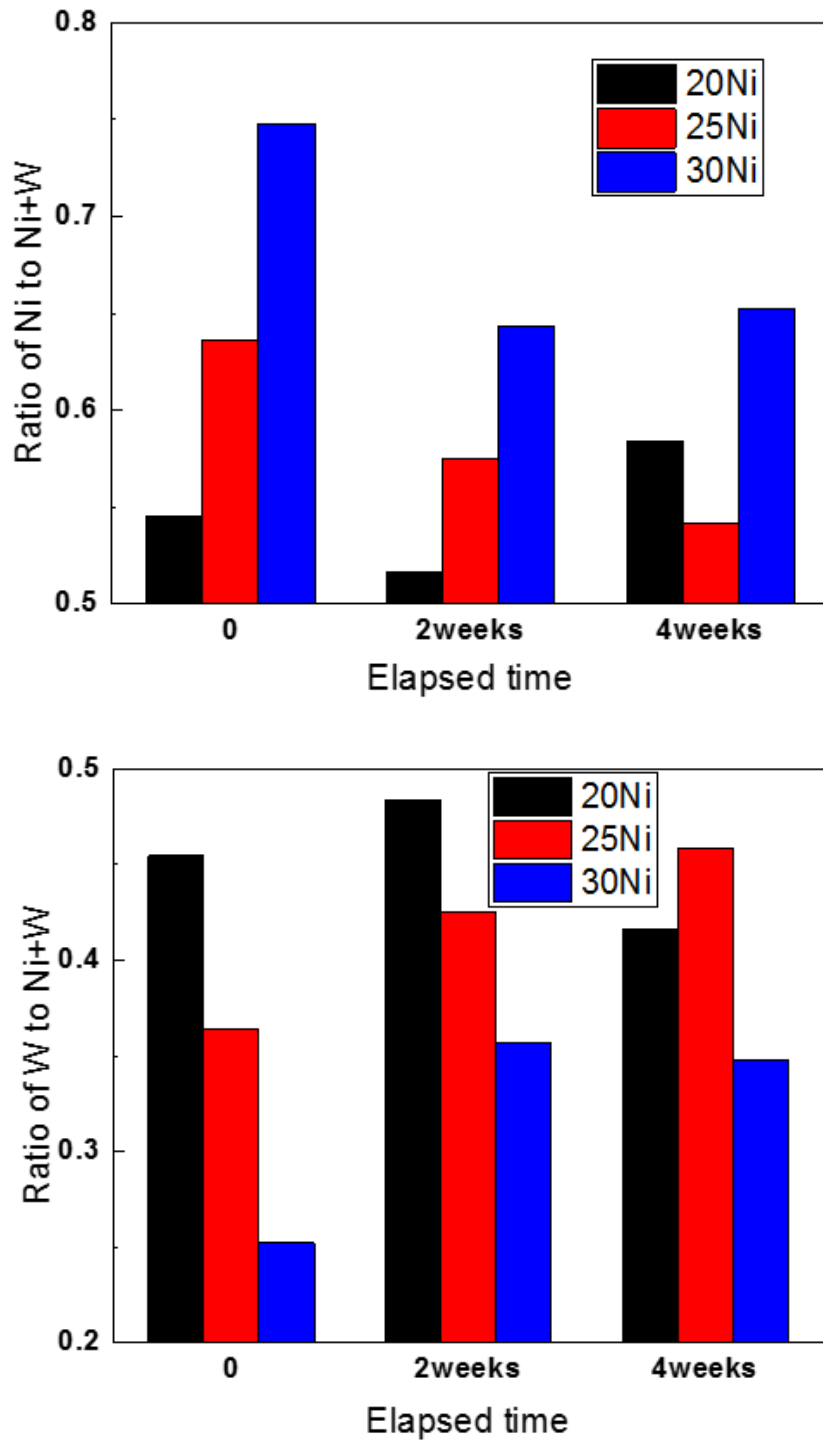
Fig. 6.2 The proportion of Ni and W before and after FAC simulation experiments

(a)

(b)

(c)
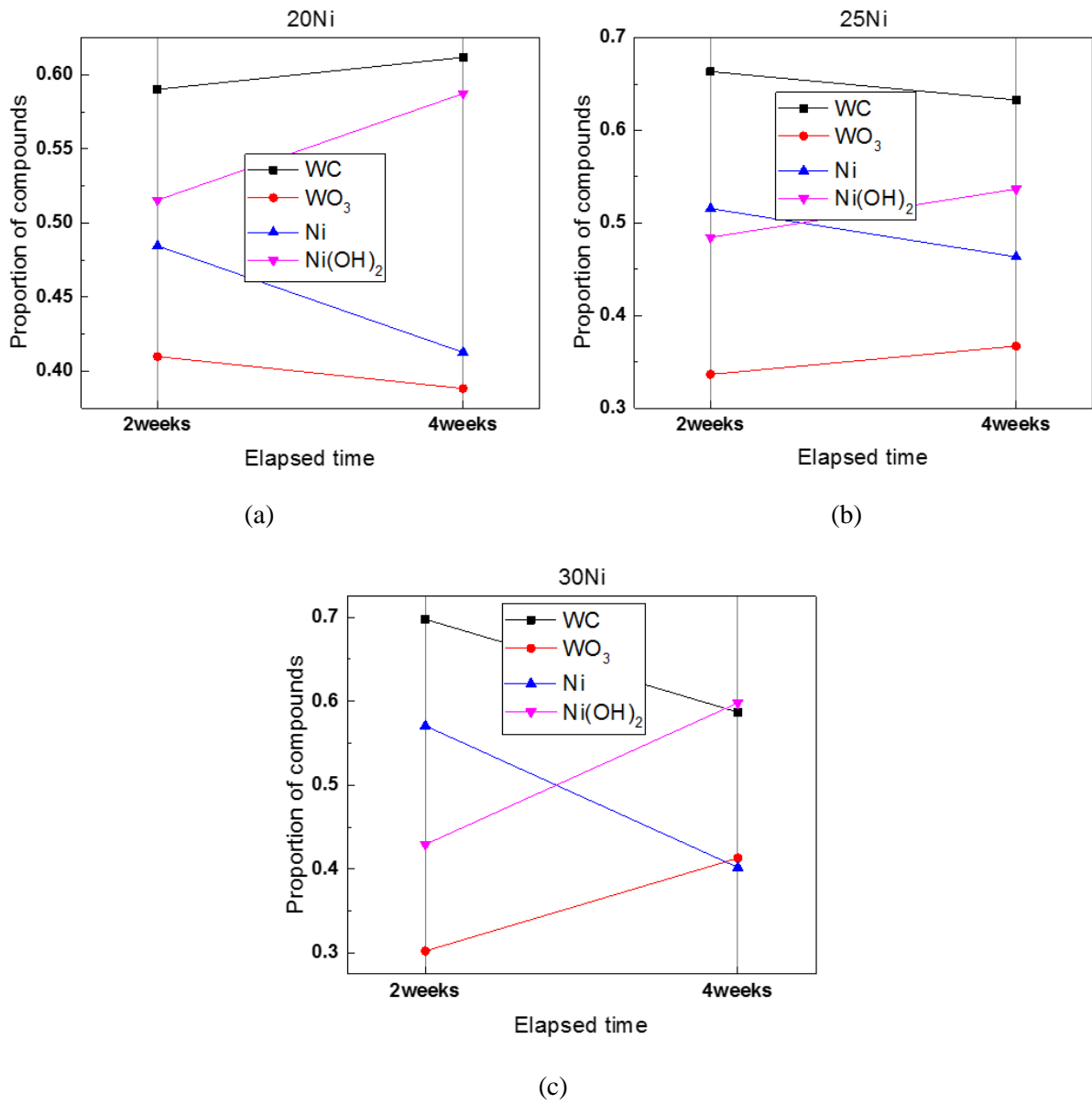
Fig. 6.3 The proportion of the compounds of coating (a: 20Ni, b: 25Ni and c: 30Ni coating)
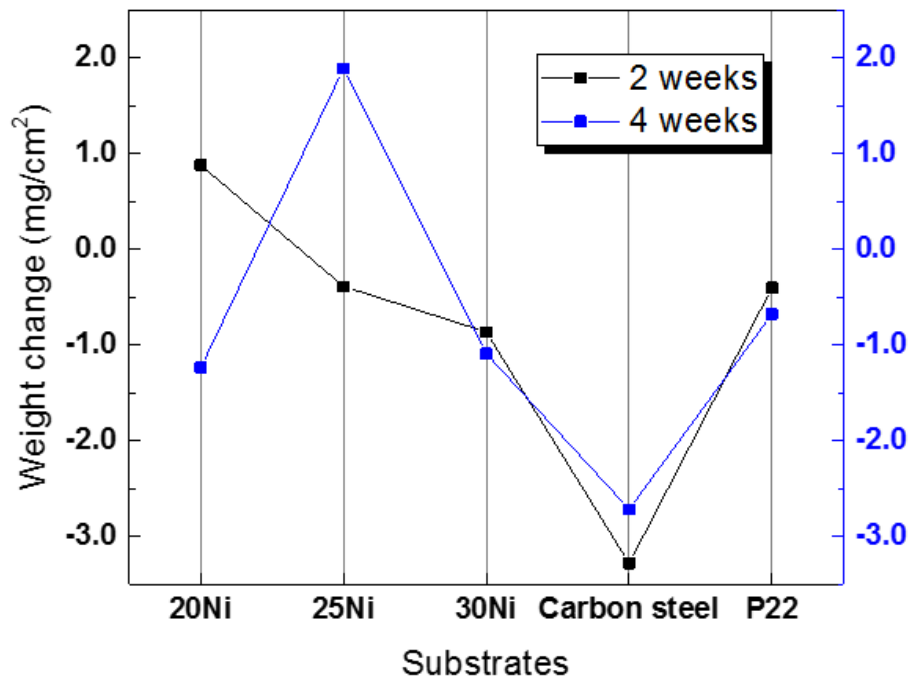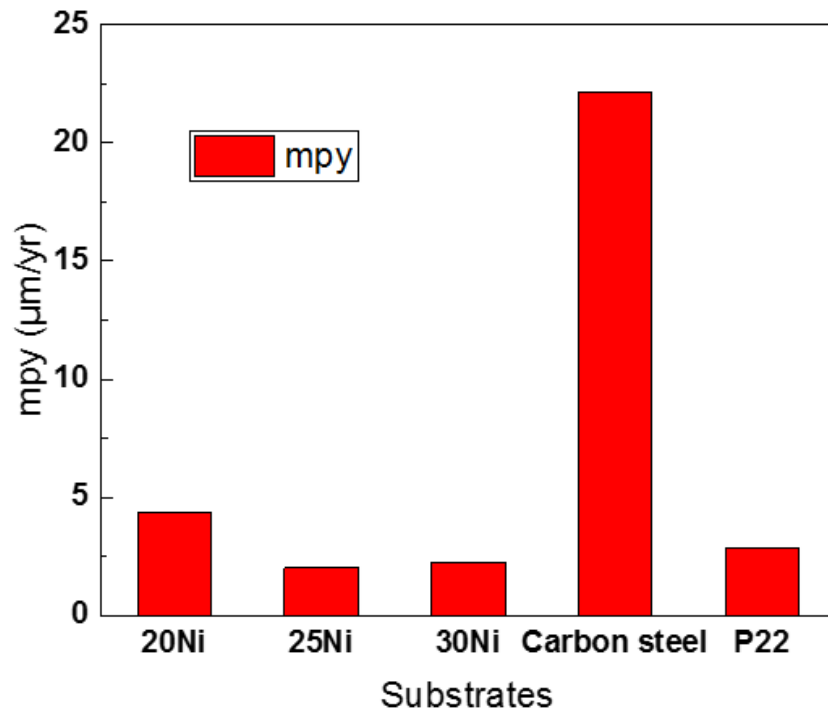
Fig. 6.4 Mpy of specimens and weight change after FAC simulation experiments

VII. Conclusion

For application to secondary piping system of nuclear power plant, corrosion behavior of cold sprayed WC-Ni coatings is evaluated *via* potentiodynamic polarization at room temperature and FAC simulation experiments at high temperature (150 °C) during 2 weeks and 4 weeks.

From experimental results and study, the following results can be obtained.

1. During cold spray coating, oxide products or other decarburized components are not observed at coating surface which is the intrinsic characteristic of cold spray coating. Compressed air can be used because it does not generate oxidation or decarburization of powder.

2. Dissolution of binder metal at WC-Ni coating is observed and a tendency of weight change of coating with time is different by Ni contents. At early stage of corrosion, weight gain occurs from 20Ni but weight loss is increased with increasing Ni contents. However, weight of 25Ni coating is increased and weight loss occurs at 20Ni and 30Ni coating after 4 weeks.

3. Different tendency of weight change is caused by galvanic corrosion of Ni caused by low reduction potential of Ni. Moreover, the thermal stability of $Ni(OH)_2$ induces different results of coating.

4. Lower Ni contents than 25Ni coating such as 20Ni coating reduces galvanic corrosion of Ni and induces WC dissolution. Although higher Ni contents than 25Ni coating such as 30Ni coating can protect corrosion of WC, low WC contents and high dissolution of $Ni(OH)_2$ in coating influence on weight loss.

5. WC-10Ni + 25Ni has better corrosion properties by results from potentiodynamic polarization and FAC simulation experiments. Therefore, WC-10Ni + 25Ni coating is possibly suggested to one of option to reducing corrosion of carbon steel.

Reference

[1]   Cattant, F., Crusset, D., & Féron, D. (2008). Corrosion issues in nuclear industry today. Materials today, 11(10), 32-37.

[2]   Jones, D. A. (1992). Principles and prevention of corrosion. Macmillan.

[3]   Ahmed, W. H. (2012). Flow accelerated corrosion in nuclear power plants. INTECH Open Access Publisher.

[4]   Machiels, A. (2006). Recommendations for an effective Flow-Accelerated Corrosion Program (NSAC-202L-R3). EPRI TR-1011838, Electric Power Research Institute.

[5]   Kain, V. (2014). Flow accelerated corrosion: forms, mechanisms and case studies. Procedia Engineering, 86, 576-588.

[6]   Beverskog, B., & Puigdomenech, I. (1996). Revised Pourbaix diagrams for iron at 25–300 C. Corrosion Science, 38(12), 2121-2135.

[7]   Ahmed, W. H. (2012). Flow accelerated corrosion in nuclear power plants. INTECH Open Access Publisher.

[8]   Kain, V., Roychowdhury, S., Ahmedabadi, P., & Barua, D. K. (2011). Flow accelerated corrosion: Experience from examination of components from nuclear power plants. Engineering Failure Analysis, 18(8), 2028-2041.

[9]   Pietralik, J. M. (2012). The role of flow in flow-accelerated corrosion under nuclear power plant conditions. EJ Adv Maint, 4, 63-78.

[10]   Betova, I., Bojinov, M., & Saario, T. (2010). Predictive modeling of flow-accelerated corrosion– unresolved problems and issues. VTT research report No VTT-R-08125-10.

[11]   Scheers, P. V. (1992). The effects of flow velocity and pH on the corrosion rate of mild steel in a synthetic minewater. Journal of the South African Institute of Mining and Metallurgy(South Africa), 92(10), 275-281.

[12]   Jingjun, L., Yuzhen, L., & Xiaoyu, L. (2008). Numerical simulation for carbon steel flow-induced corrosion in high-velocity flow seawater. Anti-Corrosion Methods and Materials, 55(2), 66-72.

[13]   Giddey, S., Cherry, B., Lawson, F., & Forsyth, M. (2001). Stability of oxide films formed on mild steel in turbulent flow conditions of alkaline solutions at elevated temperatures. Corrosion science, 43(8), 1497-1517.

[14]   Fujiwara, K., Domae, M., Yoneda, K., & Inada, F. (2011). Model of physico-chemical effect on flow accelerated corrosion in power plant. Corrosion Science, 53(11), 3526-3533.

[15]   Remy, F. N., & Bouchacourt, M. (1992). Flow-assisted corrosion: a method to avoid damage. Nuclear Engineering and design, 133(1), 23-30.

[16]   Satoh, T., Shao, Y., Cook, W. G., Lister, D. H., & Uchida, S. (2007). Flow-assisted corrosion of carbon steel under neutral water conditions. Corrosion, 63(8), 770-780.

[17]   Evgeny, B., Hughes, T., & Eskin, D. (2016). Effect of surface roughness on corrosion behaviour of low carbon steel in inhibited 4M hydrochloric acid under laminar and turbulent flow conditions. Corrosion Science, 103, 196-205.

[18] Brett, C., Brett, M. O., Brett, A. M. C. M., & Brett, A. M. O. (1993). Electrochemistry: principles, methods, and applications (No. 544.6 BRE).

[19] Pawlowski, L. (2008). The science and engineering of thermal spray coatings. John Wiley & Sons.

[20] Davis, J. R. (Ed.). (2004). Handbook of thermal spray technology. ASM international.

[21] Assadi, H., Gärtner, F., Stoltenhoff, T., & Kreye, H. (2003). Bonding mechanism in cold gas spraying. Acta Materialia, 51(15), 4379-4394.

[22] Papyrin, A., Kosarev, V., Klinkov, S., Alkhimov, A., & Fomin, V. M. (2006). Cold spray technology. Elsevier.

[23] Schmidt, T., Gärtner, F., Assadi, H., & Kreye, H. (2006). Development of a generalized parameter window for cold spray deposition. Acta materialia, 54(3), 729-742.

[24] Guilemany, J. M., Fernandez, J., Delgado, J., Benedetti, A. V., & Climent, F. (2002). Effects of thickness coating on the electrochemical behaviour of thermal spray Cr_3C_2–NiCr coatings. Surface and coatings technology, 153(2), 107-113.

[25] Takeda, M., Morihiro, N., Ebara, R., Harada, Y., Wang, R., & Kido, M. (2002). Corrosion Behavior of Thermally Sprayed WC Coating in Na_2SO_4 Aqueous Solution. Materials Transactions, 43(11), 2860-2865.

[26] Hong, S., Wu, Y., Zheng, Y., Wang, B., Gao, W., & Lin, J. (2013). Microstructure and electrochemical properties of nanostructured WC–10Co–4Cr coating prepared by HVOF spraying. Surface and Coatings Technology, 235, 582-588.

[27] Kear, B. H., Skandan, G., & Sadangi, R. K. (2001). Factors controlling decarburization in HVOF sprayed nano-WC/Co hardcoatings. Scripta Materialia, 44(8), 1703-1707.

[28] Richert, M. W., Mikulowski, B., Palka, P., & Perek-Nowak, M. (2013). The Effect of Chemical Composition and Thermal Sprayed Method on the Chromium and Tungsten Carbides Coatings Microstructure.

[29] Couto, M., Dosta, S., & Guilemany, J. M. (2015). Comparison of the mechanical and electrochemical properties of WC-17 and 12Co coatings onto Al7075-T6 obtained by high velocity oxy-fuel and cold gas spraying. Surface and Coatings Technology, 268, 180-189.

[30] Dosta, S., Couto, M., & Guilemany, J. M. (2013). Cold spray deposition of a WC-25Co cermet onto Al7075-T6 and carbon steel substrates. Acta Materialia, 61(2), 643-652.

[31] Couto, M., Dosta, S., Torrell, M., Fernández, J., & Guilemany, J. M. (2013). Cold spray deposition of WC–17 and 12Co cermets onto aluminum. Surface and Coatings Technology, 235, 54-61.

[32] Gubisch, M., Liu, Y., Krischok, S., Ecke, G., Spiess, L., Schaefer, J. A., & Knedlik, C. (2005). Tribological characteristics of WC_{1-x}, W_2C and WC tungsten carbide films. Tribology and Interface Engineering Series, 48, 409-417.

[33] Sathish, S., Geetha, M., & Asokamani, R. (2014). Comparative Studies on the Corrosion and Scratchbehaviors of Plasma Sprayed ZrO_2 and WC-Co Coatings. Procedia Materials Science, 6, 1489-1494.

[34] Voitovich, V. B., Sverdel, V. V., Voitovich, R. F., & Golovko, E. I. (1996). Oxidation of WC-Co, WC-Ni and WC-Co-Ni hard metals in the temperature range 500–800 C. International Journal of Refractory Metals and Hard Materials, 14(4), 289-295.

[35] Hochstrasser-Kurz, S. (2006). Mechanistic study of the corrosion reactions on WC-Co

hardmetal in aqueous solution-An investigation by electrochemical methods and elemental solution analysis. Diss., Eidgenössische Technische Hochschule ETH Zürich, Nr. 16535, 2006.

[36] Ismail, A., & Abd Aziz, N. (2014). Corrosion behavior of WC-Co and WC-Ni in 3.5% NaCl at increasing temperature. Applied Mechanics and Materials, 660, 135-139.

[37] Weidman, M. C., Esposito, D. V., Hsu, I. J., & Chen, J. G. (2010). Electrochemical stability of tungsten and tungsten monocarbide (WC) over wide pH and potential ranges. Journal of the Electrochemical Society, 157(12), F179-F188.

[38] Weidman, M. C., Esposito, D. V., Hsu, Y. C., & Chen, J. G. (2012). Comparison of electrochemical stability of transition metal carbides (WC, W_2C, Mo_2C) over a wide pH range. Journal of Power Sources, 202, 11-17.

[39] Alsabet, M., Grden, M., & Jerkiewicz, G. (2011). Electrochemical Growth of Surface Oxides on Nickel. Part 1: Formation of α-NiOOH in Relation to the Polarization Potential, Polarization Time, and Temperature. Electrocatalysis, 2(2), 317-330.

[40] Alsabet, M., Grden, M., & Jerkiewicz, G. (2014). Electrochemical Growth of Surface Oxides on Nickel. Part 2: Formation of β-Ni $(OH)_2$ and NiO in Relation to the Polarization Potential, Polarization Time, and Temperature. Electrocatalysis, 5(2), 136-147.

[41] Alsabet, M., Grdeń, M., & Jerkiewicz, G. (2015). Electrochemical growth of surface oxides on nickel. Part 3: Formation of β-NiOOH in relation to the polarization potential, polarization time, and temperature. Electrocatalysis, 6(1), 60-71.

[42] Kellner, F. J. J., Hildebrand, H., & Virtanen, S. (2009). Effect of WC grain size on the corrosion behavior of WC–Co based hardmetals in alkaline solutions. International Journal of Refractory Metals and Hard Materials, 27(4), 806-812.

[43] Zhang, L., Chen, Y., Wan, Q. L., Liu, T., Zhu, J. F., & Tian, W. (2016). Electrochemical corrosion behaviors of straight WC–Co alloys: Exclusive variation in grain sizes and aggressive media. International Journal of Refractory Metals and Hard Materials, 57, 70-77.

[44] Lioma, D., Sacks, N., & Botef, I. (2015). Cold gas dynamic spraying of WC–Ni cemented carbide coatings. International Journal of Refractory Metals and Hard Materials, 49, 365-373.

[45] Latif, S., Mehmood, M., Ahmad, J., Aslam, M., Ahmed, M., & Zhang, Z. D. (2010). Ni–WC composite coatings by carburizing electrodeposited amorphous and nanocrystalline Ni–W alloys. Applied Surface Science, 256(10), 3098-3106.

[46] Ziemniak, S. E., & Goyette, M. A. (2004). Nickel (II) oxide solubility and phase stability in high temperature aqueous solutions. Journal of solution chemistry, 33(9), 1135-1159.

[47] Human, A. M., & Exner, H. E. (1996). Electrochemical behaviour of tungsten-carbide hardmetals. Materials Science and Engineering: A, 209(1), 180-191.

[48] Andersson, K. M., & Bergström, L. (2000). Oxidation and dissolution of tungsten carbide powder in water. International Journal of Refractory Metals and Hard Materials, 18(2), 121-129.

[49] Chen, L., Yi, D., Wang, B., Liu, H., & Wu, C. (2016). Mechanism of the early stages of oxidation of WC–Co cemented carbides. Corrosion Science, 103, 75-87.

Acknowledgement

2년동안의 석사과정을 마무리하면서 전하지 못한 감사의 말을 마지막 이 글을 통해서 전하고자 합니다. 원자력에 대해서 많은 것을 알지 못함에도 불구하고 UNIST에 대학원생으로 입학하고 나서 계속해서 저를 지도해주신 저의 지도교수님, 김지현 교수님을 비롯하여, 마지막까지 저에게 연구결과뿐만 아니라 석사과정 이후의 일까지 많은 조언을 해주신 석사논문 심사위원이셨던 안상준 교수님과 최성열 교수님께 감사의 말씀을 전하고 싶습니다.

또한 다른 후배들과 다르게 자신들보다 나이가 많은 후배를 데리고 다니게 되었던 저희 연구실 대학원생들인 김태호, 김승현, 최상일, 고광범, 유승창, 이정현 대학원생들에게 항상 고마웠다고 말하고 싶습니다. 후배임에도 불구하고 자신들보다 형이라서 제대로 지적도 못한 부분도 많을 것이고, 연구실 내부에서의 생활에서도 답답한 부분이 많았을 것이라고 생각합니다. 각각을 개인별로 전부다 언급할 수는 없지만 특히 제 사수였던 김승현 대학원생에게는 항상 미안한 마음이 먼저 들어서인지 서로가 조심스러웠던 것 같습니다. 하지만 연구실 대학원생들에게 연구나, 대학원 공부에서 정말 많은 도움을 받았고 그로 인해서 무사히 마칠 수 있었습니다. 또한 저와 같은 또래인 최경준 대학원생은 제가 들어온 이후 연구실에 적응하기 위해 선배로서 좋은 말도 해주고 친구로서 따끔한 말도 많이 해주어 마지막까지 대학원생활을 즐겁게 마무리할 수 있었습니다. 대학생시절, 처음 이곳의 연구실을 소개받을 때 자신의 연구와 연구실을 소개시켜주신, 지금은 졸업하고 안 계시는 신상훈 선배님께 감사하다고 전해드리고 싶습니다. 제가 들어온 이후로 대학원생으로 들어온 함준혁, 김태용, 송인영 대학원생에게는 많은 것을 알려주지 못했고 오히려 제가 배운 것이 많아 감사하게 생각합니다.

지금까지 제가 행한 모든 일들을 가능하게 해 주시고 아들에게 변함없이 베풀어주셨던 저를 이 세상에 나오게 만들어주신 아버님, 어머님께 말로서는 표현하지 못할 존경을 보냅니다. 제가 힘들고 어려울 때 옆에서 지켜봐 주셨고 그 덕분에 여기까지 올 수 있었습니다. 그리고 제가 가장 아끼는 우리 동생, 지금까지 잘해왔고 이제부터는 좋은 일만 가득할 거라고 말해주고 싶습니다.

마지막으로 이 연구를 가능하게 한 모든 분들께 감사의 말을 전합니다.

감사합니다.